The Effect of Favourable and Unfavourable Frost on Air Cooling Coil Performance

A thesis presented in partial fulfilment of the requirements for the Degree of Master of Technology, at Massey University.

Antony Noel O'Hagan
B.Tech. (Hon) (Ind.Tech.)

1994

ABSTRACT

The most common type of air cooling coil used in the refrigeration industry is the finned tube heat exchanger. The performance of such coils can be greatly hindered by frost formation, which will occur when the coil surface temperature is both below the dewpoint of the air passing over it, and below 0°C. Frost reduces performance, both through the increased thermal resistance of the frost layer, and by reduction of the air flow through the coil.

Whilst frosting on coils is influential on performance, there is comparatively little information available on the performance of finned tube heat exchangers under frosting conditions. Smith (1989) has proposed an "unfavourable" frost formation theory. The theory states that unfavourable frost formation occurs when the line representing the temperature and humidity of the air passing through the coil, crosses the saturation line of the psychrometric chart. This criteria is more likely to occur under conditions of high relative humidity, low sensible heat ratio (*SHR*), and/or high refrigerant-to-air temperature difference (*TD*). Under unfavourable conditions it is suggested that the frost will be of particularly low density, which would cause coil performance to decline to a much greater extent for the same total frost accumulation, than under "favourable" frosting conditions.

The objectives of this study were to measure the change in performance of a cooling coil under frosting conditions, and to assess the validity of the unfavourable frost formation theory.

A calorimeter style coil test facility was used, that allowed coil performance to be measured as frost accumulated in a manner consistent with coil operation in industrial practice (i.e. declining air flowrate and a wide range of *SHR's*). The data collected supported the concept of unfavourable frost formation with a more rapid decline in performance for operation with low *SHR*, than that at high *SHR*, for the same total frost accumulation. Some recovery of coil performance was observed when operation

at low *SHR* (with rapid performance deterioration) was followed by a period of high *SHR* operation.

Equations were developed that allowed the theoretical conditions for the formation from favourable to unfavourable frosting to be quantified. The measured change in the rate of coil performance deterioration with frost buildup was dependent on air and coil conditions, in a manner consistent with these equations. The transition between favourable and unfavourable frost formation appeared to be related to the lowest temperature on the coil surface rather than the mean surface temperature. Satisfactory predictions of frost formation types were obtained by using the refrigerant evaporation temperature as an approximation to the lowest coil surface temperature.

ACKNOWLEDGEMENTS

The author would like to thank the following people for their assistance during the course of this project:

Dr Donald Cleland, Department of Process and Environmental Technology, Chief Supervisor.

Dr Andrew Cleland, Department of Process and Environmental Technology, Supervisor.

Mr John Jenkins, Steelfort Engineering Company Ltd.

Mr Wayne Sims, Steelfort Engineering Company Ltd.

Mr Keith Stocker, Steelfort Engineering Company Ltd.

The author would like to thank the following people for their patiences and technical assistance required during the experimental phase of this project:

Mr John Alger, Technical Officer, Department of Process and Environmental Technology.

Mr Wayne Mallet, Technician, Department of Process and Environmental Technology.

Mr Bruce Collins, Technician, Department of Process and Environmental Technology.

The author would like to thank the following organisations for their financial support of this project, without which this project would not have been be possible:

Technology for Business Growth Fund of the Foundation for Research, Science, and Technology.

Steelfort Engineering Company Ltd.

New Zealand Apple and Pear Marketing Board.

TABLE OF CONTENTS

LIST OF FIGURES

LIST OF TABLES

1 INTRODUCTION

The preservation of perishable food items for storage, transport, and distribution to the consumer is important, especially with seasonal production of many products, and international trade now being common place. Refrigeration is a common method of food preservation. Cost-effective refrigeration is particularly important to New Zealand, as a country whose economy is highly dependent on exports of primary products.

The most common refrigeration systems used are mechanical vapour compression units, with air as the heat transfer medium between the cooling refrigerant and the product. Air cooling coils are one of the key components used in such a system. The cooling coil, and associated fans, have two main purposes:

- provide the rate of heat transfer necessary to maintain the desired air and product temperatures, and
- provide the desired air movement through the coil, around the application, and over the product.

In some applications an additional role of maintaining the desired relative humidity of the air is also required.

Operation below 0°C can result in frost formation on the coil surface. Frost formation reduces coil performance through both insulation of the coil surface and reduced airflow through the coil. The coil must be periodically defrosted when performance becomes inadequate. All of these factors result in additional operating and capital costs for the refrigeration system, and potential disruption to the continuous operation of the application.

Prediction of the effect of frost on coil performance is important for cost-effective coil, and refrigeration system, design and operation. Although the mechanism of frost growth has been extensively researched, and good models for dry coil performance are available, there is comparatively little information on the effects of frost on air cooling coil performance. A better understanding of the factors affecting

frosted coil performance will enable costs to be minimised and plant performance to be optimised. This would represent an important step in achieving a cost-effective refrigeration system. This study into the effect of frost on air cooling coil performance is therefore clearly justified.

2 LITERATURE REVIEW

2.1 INTRODUCTION

The most common type of air cooling coil used in the refrigeration industry is the finned tube heat exchanger. The finned tube heat exchanger comprises of a bank of horizontal tubes with either continuous fin sheets or individual fins, perpendicular to the tubes. Usually fans are associated with the coil, and provide air flow parallel to the fins, and across the tubes. The cooling refrigerant is circulated inside the tubes. A wide variety of coil configurations are possible including: forced or induced draught air flow; fixed or variable speed fans; direct expansion, flooded, or pumped refrigerant circulation; counter-current, co-current, or cross-flow refrigerant to air arrangements; staggered or in-line tube alignment; single or multiple refrigerant circuits; variable or uniform fin spacing; collared or welded fins; flat or wavy fins; and a number of possible materials of construction.

The performance of such coils can be greatly hindered by frost formation, which will occur when the coil surface temperature is both below the dewpoint of the air passing over it, and below 0°C. Frost reduces coil performance, both through the increased thermal resistance of the frost layer, and by reduction of the air flow through the coil (Sanders, 1974; Kondepudi & O'Neal, 1987; Stoecker, 1988). With frost formation the refrigeration system must either operate with a lower refrigerant evaporation temperature to compensate for the loss of performance, or there may be loss of temperature control in the application. The reduction in air flowrate can also have important effects on uniformity of conditions in the refrigerated room, and on the desired heat transfer in the room, such as removal of heat from product. In addition, the coil must be periodically defrosted when performance becomes unsatisfactory, incurring further energy costs, and disrupting operation of the application. A better understanding of the mechanisms of frost formation, and its impact on coil heat transfer, is important to designers and operators of refrigeration systems.

A significant amount of literature is available in the heat transfer and frost growth

field. For practical reasons, this review was limited to papers that met one or more of the following criteria:

- they considered finned tube heat exchangers with evaporating refrigerant as the coolant; other geometries and configurations are only discussed if the principles involved are more generally applicable,
- they describe physical models for, or measurements of, frost formation where these aid in the understanding of the performance of the coil,
- they contain mathematical models of coil performance that are macroscopic, rather than microscopic in nature, and
- they describe coil performance measurement methods and standards relevant to finned tube heat exchangers.

The literature can be divided into several broad categories;

- cooling coil performance under dry conditions,
- measurement and modelling of frost formation, frost growth and frost properties,
- frosted coil performance measurements, and
- models of coil performance with frosting.

The basic equations describing instantaneous cooling coil heat transfer rates are presented first as a framework for further discussion of the literature.

2.2 INSTANTANEOUS COIL HEAT TRANSFER RATES

The following equations describe the instantaneous rate of heat transfer for a cooling coil in terms of the air-on and air-off conditions. The total rate of heat transfer is the sum of the sensible and latent components. Sufficient accuracy for industrial situations is achieved with the following definitions:

$$\phi_t = \phi_s + \phi_l \qquad (2.1)$$

$$\phi_s = m_a\, c_a\, (T_{on} - T_{off}) \tag{2.2}$$

$$\phi_l \approx m_a\, \Delta h\, (H_{on} - H_{off}) \tag{2.3}$$

where:

ϕ_t = total coil heat transfer rate (W)

ϕ_s = coil sensible heat transfer rate (W)

ϕ_l = coil latent heat transfer rate (W)

m_a = mass flowrate of dry air (kg/s)

c_a = specific heat capacity of dry air (J/kg)

T_{on} = coil air-on temperature (°C)

T_{off} = coil air-off temperature (°C)

Δh = latent heat of condensation or sublimation of water vapour (J/kg)

H_{on} = coil air-on absolute humidity (kg/kg)

H_{off} = coil air-off absolute humidity (kg/kg)

The total heat transfer rate can also be expressed in terms of the sensible heat load and the sensible heat ratio (*SHR*), or using the reciprocal of *SHR*, the total to sensible ratio (*T:S*):

$$\phi_t = \frac{\phi_s}{SHR} = \phi_s\, T{:}S \tag{2.4}$$

These equations alone cannot be used to model the cooling coil heat transfer performance, because the air-off conditions cannot be predicted without *a priori* knowledge of the physical characteristics of the coil, the air-on conditions, and refrigerant conditions. The normal approach is to predict ϕ_s and ϕ_l separately, (or ϕ_s and either *SHR* or *T:S*).

2.3 DRY COOLING COIL PERFORMANCE MODELS

Under moisture free conditions there is no condensation or frost formation, there is no latent component, and consequently only the sensible heat transfer needs to be considered. The standard approach is to ignore transient effects and use a quasi-steady-state approach. Dynamic models are generally only used in the specialised field of dynamic simulation of refrigeration systems (Cleland, 1990).

2.3.1 Sensible Heat Capacity Rating

Commonly, the sensible heat transfer is described by an overall sensible capacity rating for the coil. This can be expressed in terms of the mean temperature difference between the air and the refrigerant:

$$\phi_s = U\ A\ TD_m \tag{2.5}$$

where: U = overall sensible heat transfer coefficient ($W/m^2{}^oC$)

A = coil surface area (m^2)

TD_m = mean temperature difference between the refrigerant and the air (°C).

U and A are usually grouped together as the sensible heat transfer rating for the coil, UA. For countercurrent flow of an evaporating refrigerant with minimal refrigerant side pressure drop, the mean temperature difference between the refrigerant and the air, is defined as (Stoecker, 1988; Cleland and Cleland, 1992):

$$TD_m = \frac{(T_{on} - T_{re}) - (T_{off} - T_{re})}{\ln\left[\dfrac{T_{on} - T_{re}}{T_{off} - T_{re}}\right]} \tag{2.6}$$

where: T_{re} = refrigerant evaporation temperature (°C)

Alternatively, the air-on temperature difference between the air and the refrigerant

can be used:

$$\phi_s = UA_{on}(T_{on} - T_{re}) \tag{2.7}$$

where: UA_{on} = air-on coil sensible performance rating (W/°C).

The relationship between the alternative capacity ratings is (Stoecker, 1988):

$$UA_{on} = m_a\, c_a\, (1 - \exp^{\frac{-UA}{m_a c_a}}) \tag{2.8}$$

The overall heat transfer coefficient, UA, represents the combined effect of refrigerant and air-side heat transfer coefficients, fin area and efficiency, and tube area and conductivity. This can be described by (Stoecker & Jones, 1982):

$$\frac{1}{UA} = \frac{1}{h_a(\eta A_f + A_a)} + \frac{1}{h_r A_r} + \frac{x}{\lambda A_m} \tag{2.9}$$

where:

λ	=	thermal conductivity of the tubes (W/m°C)
η	=	fin efficiency
A_a	=	air-side area of the tubes (m^2)
A_f	=	fin surface area (m^2)
A_m	=	mean area of the tubes (m^2)
A_r	=	refrigerant side area of the tubes (m^2)
h_a	=	heat transfer coefficient on the air side ($W/m^2\,°C$)
h_r	=	heat transfer coefficient on the refrigerant side ($W/m^2\,°C$)
x	=	tube thickness (m)

The first term on the right hand side is the air-side and fin heat transfer resistance, the second is refrigerant side heat transfer resistance, and the third represents conduction through the tube wall. The conduction term is often omitted, because it is usually negligible.

2.3.2 Capacity Rating Component Models

A large number of papers have considered the prediction of refrigerant side heat transfer coefficients for evaporation of refrigerant in tubes. Recent reviews of correlations relevant to finned tube heat exchangers are given by Turaga and Guy (1985) and Pate (1992). Prediction of refrigerant side heat transfer coefficients is not simple due to the presence of two-phase flow, changing refrigerant quality through the coil, the presence of lubricating oil, and presence of a superheating region for direct expansion coils (Shah, 1976; Stoecker and Jones, 1982; Turaga and Guy, 1985). Most correlations used for coils are functions of heat flux, mass flux, and refrigerant properties.

Similarly, a large number of papers have considered air-side heat transfer coefficients for configurations relevant to finned tube heat exchangers. Reviews of prediction methods are given by Sanders (1974) and Webb (1980). Many correlations are empirical in nature and therefore are specific to the type and geometry of the heat exchanger studied and to the test conditions used. Most are based on measurements without frost present.

Fin efficiency is the ratio of actual fin-to-air heat transfer, to that if the entire fin was at the primary surface temperature. Incorporating such a term eliminates the difficulty of different surface temperatures across the coil, and can allow for non-ideal contact between the fins, and the tubes (Kondepudi and O'Neal, 1987). A number of relationships and charts, for fin efficiency, for different fin geometries are available (Stoecker and Jones, 1982; Sanders, 1974). Kays and London (1964) developed a commonly used relationship for fin efficiency for a flat plate, in terms of the fin geometry, thermal conductivity, and air-side heat transfer coefficient.

2.3.3 Overall Coil Heat Transfer Models

Refrigerant and air-side heat transfer coefficients can change substantially throughout a coil due to changes in refrigerant quality, air to refrigerant temperature differences,

pressure drops etc. Frequently average values for the entire coil are used rather than integrating the changes in conditions over the entire coil. Yamagishi and Karaki (1975), Goldstein (1983), Hauhas (1983), Domanski and Didion (1984), Poroedos and Gaspersic (1987), and Nesjie and Skaugen (1989) all present overall air coil models that are based on steady-state section-by-section analyses of the coil. None of these included the effect of frost formation. Goldstein (1983) and Nesjie and Skaugen (1989) allowed for the latent heat transfer due to condensation (wet conditions) as this can be analyzed in a steady-state manner.

2.4 FROST GROWTH AND FROST PROPERTIES

2.4.1 Frost Growth

In order in predict the macroscopic effects of frost on coil performance, it is useful to first consider the microscopic process involved in frost formation and growth.

The process of frost formation and growth is a cumulative and continuously changing situation, making it difficult to predict frost characteristics, and prevents any steady state analysis (Jones and Parker, 1975). Frost parameters such as density, thermal conductivity, and thickness which are highly influential in the effect of frost on coil performance, are dependent not only on the conditions under which frost is forming, but also time and the history of how the frost was formed (Jones and Parker, 1975).

The frost formation process can be divided into three periods; crystal growth, frost layer growth, and finally, frost layer full growth period (Hayashi *et al*, 1977). Initially ice crystal nucleation must occur, which is a somewhat random process. The individual frost crystals grow independently, in a vertical direction, to form a thin frost layer. From this cluster, usually of rod type crystals, individual crystals branch and begin to interact, and the frost layer growth period begins. The frost layer becomes more uniform and the frost density begins to increase. At this point the water vapour at the frost surface can take two paths. It can diffuse into the frost

layer and increase the frost density, or can increase the frost thickness at the surface (Jones and Parker, 1975). In practice both processes would occur simultaneously. At temperatures close to 0°C the increased thermal resistance may result in the frost surface melting, and the condensate soaking into, and freezing, within the frost layer (Hayashi *et al*, 1977). During the full growth period the frost density would be expected to increase further, along with addition to frost thickness.

2.4.2 Frost Properties and Heat Transfer in Simple Geometries

O'Neal and Tree (1985) reviewed frost formation in simple geometries. This review was divided into three categories; frost properties, frost growth in simple geometries, and heat transfer in simple geometries. Two of the important frost properties for frost growth and heat transfer modelling are the frost density and thermal conductivity. Both can change by an order of magnitude as frosting proceeds.

Frost density has been observed to initially decrease, followed by a steady increase (Hayashi *et al*, 1977). Hosoda and Uzuhashi (1967) observed frost densities ranging from 60 to 600 kg/m^3, Lotz (1971) from 20 to 400 kg/m^3, and Gatchilov and Ivanova (1979) observed densities from 20 to 250 kg/m^3.

There is wide variation in the correlations between thermal conductivity and frost density, probably due to differences in the crystal structure and porosity of the frost. Correlations between density and thermal conductivity showed that as density increased, there was a corresponding increase in thermal conductivity (Hosoda and Uzuhashi, 1967; O'Neal and Tree, 1985). The structure of frost formed under one set of conditions can be dramatically different to that under another set of conditions. Any correlation should only be used within the range of conditions for which it was defined. Some frost thermal conductivity correlations also include terms for frost and/or surface temperatures (Brian et al 1969; Marinyuk, 1980).

Frost growth has been studied on a number of simple geometries, including cylinders, flat plates, through annulus, and in parallel plates. The major variables affecting

frost growth appeared to be air velocity, surface temperature, location, and air humidity. Increased frost thickness was encountered with a decrease in wall or surface temperature, and with increased humidity (Hosoda and Uzuhashi, 1967; O'Neal and Tree, 1985). Not all investigations agree on the impact of air velocity (or Reynolds number) on the rate of frost growth. Schneider (1978) found frost growth to be independent of Reynolds number, while Hosoda and Uzuhashi (1967) found it to be dependent. O'Neal and Tree (1985) suggest that there may be a critical Reynolds number, above which frost growth is independent of Reynolds number (15900 for flow through a parallel plate heat exchanger). They stated that theoretically the frost at the leading edge should be thicker than that at the rear, as the heat and mass transfer coefficients are greater at the front. This appeared true in some situations, however in other situations uniform frost growth was experienced. O'Neal and Tree (1985) commented that this effect has not been adequately quantified.

Kamai *et al* (1952), Chung and Algren (1953), and Hosoda and Uzuhashi (1967), found the Chilton-Colburn analogy to be applicable under frosting conditions, enabling the mass transfer coefficient to be inferred from the heat transfer coefficient and visa versa. As the frost surface is usually rougher than the surface on which it forms, the air-to-frost heat transfer coefficient is usually greater than for air-to-metal.

2.5 MEASUREMENT OF FROSTED COIL PERFORMANCE

2.5.1 Coil Testing Standards

Two available coil testing standards include performance measurement for coils operating under frosting conditions. These standards attempt to quantify average performance, but do not show how performance varies as frost forms on the coil surface.

The ASHRAE Standard 25-77 (ASHRAE, 1976) for testing coils which operate below 0°C, specifies testing under frost-free conditions. It is up to the system designer to add the required "application factor", to allow for reduced performance due to coil frost, and to compensate for lower operating times due to defrosting requirements. Under this standard, coil capacity is determined by the enthalpy change in the refrigerant across the coil, and/or the total heat inputs to a calibrated box which holds the test coil. This standard provides the definitions, required accuracy, and calculations for the testing of coils, but does not state precise test conditions, and omits testing under frosted conditions.

The Dutch air cooling coil performance testing standard (Netherlands Standard NEN 1876; Netherlands Standards Institute, 1979) requires measurement of dry performance, frosted performance, and the defrost requirements of the coil. The standard specifies a calorimeter type facility and gives 5 test conditions, with temperatures from 4°C to -30°C, and relative humidity from 80 to 85%. For each test condition, the wet and dry heat loads are adjusted to maintain the air-on temperature and relative humidity, and refrigerant evaporation temperature, at the prescribed levels. Refrigeration capacity is determined by refrigerant flow and the enthalpy difference of the refrigerant across the coil. Coil operation and heat addition is stopped, and defrosting commenced, once the coil performance has fallen below 85% of the nominal refrigeration capacity (which is that after 30 minutes of operation). Cooling coil capacity definitions are given that incorporate the effects of frosted coil performance, and defrosting losses to give a time-averaged frosted performance rating.

Sanders (1972) states that in many cases the coil capacity is not clearly defined, and can lead to dispute and controversy. The use of an average cooling capacity such as those given by the Dutch Standard was recommended. Infante-Ferriera (1988) noted the danger in using the nominal refrigeration capacity for design purposes because the actual coil performance under frosting conditions can be considerably lower.

2.5.2 Coil Performance Measurements

There are two main types of coil test facilities - calorimeter chambers, and air tunnels. Calorimeters are generally considered more representative of the true coil operating conditions, whilst the tunnel type arrangement allows air parameters to be varied to greater limits (Gatchilov and Ivanova, 1979). Sanders (1972) added that calorimeters allow testing of the complete unit, including defrost. However, there is increased possibility of non-homogeneous air conditions at coil entrance and fog formation, and greater difficulty measuring air flowrate and controlling humidity, compared to the use of wind tunnel facilities.

The two main factors affecting frosted coil performance are the reduced airflow through the coil and the insulation of the coil surface. Firstly, the frost reduces the air free flow area, which decreases the effective fin spacing. For the same total air flowrate, the reduced free flow area increases air-side pressure drop across the coil (Stoecker, 1957). Depending on the fan characteristics, the reduced free flow area may reduce the air mass flowrate, face velocity, and therefore the air-side heat transfer coefficient (Sanders, 1974). Secondly, the frost insulates the coil surface. The degree of insulation will depend on the amount of frost and the frost properties, particularly density and thermal conductivity (O'Neal and Tree, 1985).

Stoecker (1957) performed trials on finned coils with air temperature of 0°C, 72% relative humidity, fin density of 4 and 9 fins per inch (fpi), operated under constant air flow (varied between trials). Heat transfer performance was based on, U, the sensible heat transfer coefficient. Stoecker reported an initial increase in coil performance with the onset of frost formation, followed by a performance decline. The initial increase was attributed to an increase in surface roughness and surface area. The decline was considered the result of the insulation of the coil surface by the frost. It should be noted that although the airflow was constant in Stoecker's trials, the air velocity through the coil would actually increase as the coil blocked with frost, increasing the air-side heat transfer coefficient. Although the trials were at constant air flowrate, he concluded, that due to increased pressure drop, the effect

of frost on diminishing air flow was of more concern than the effect on heat transfer. Increased air flow and lower fin density lead to higher heat transfer performance. Higher pressure drops were observed at higher airflow rates. Stoecker recommended air flow as the best indication of the optimum time to defrost.

Hosoda and Uzuhashi (1967) used a tunnel test facility, with copper cooling plates, and finned tube heat exchangers. The experimental conditions were: air temperatures from 0°C to 10°C, relative humidities of 50% to 80%, and surface temperatures from -23°C to -13°C. During their trials, frost growth was observed to be uniform throughout the coil. They noted an increase in frost formation with reduced coil surface temperature and increased air velocity. Increased air velocity and higher surface temperatures produced denser, smoother, ice like frost. They gave correlations for frost density, based on surface temperature and air velocity. The air-side surface heat transfer coefficient with frost, was found to be approximately twice that of the unfrosted flat plate. This was attributed to the increased surface area.

Lotz (1971) conducted trials at air temperatures from -20°C to 0°C, and relative humidities of 40 to 80%. Heat and mass transfer coefficients were found to be higher for the frost-air interface than for the dry metal-air interface, and they increased with frost roughness. Highest frost surface roughness was produced for low air velocities, low air and wall temperatures, and low air relative humidity.

Niederer (1976) conducted trials on ammonia cooling coils at 0°C air temperature, with various fin spacings from 2 to 6 fpi (including variable spacing). The overall heat transfer coefficient was estimated, based on the mean temperature difference between refrigerant and air. At 85% relative humidity uneven frost distribution was observed, with the bulk of the frost deposited on the first rows of the coil. It was concluded that the decrease in heat transfer coefficient during frosting, was directly related to reduced air flowrate. Wider fin spacing was found to perform better under frosting conditions, as operation between defrosting was prolonged. Variable fin spacing performed better than fixed fin spacing, under the same frosting conditions.

Gatchilov and Ivanova (1975) investigated a range of air flow rates, but held air flow constant during each trial. Relative humidity was 80 to 83%, air temperature of 0°C, and temperature difference was 8°C for all trials. They found increased air flow resulted in increased frost growth, higher pressure drop, and gave greater heat transfer coefficients.

Gatchilov and Ivanova (1977) conducted trials in a calorimeter facility. They tested direct expansion finned tube heat exchangers for air temperature in the range -10°C to 0°C, relative humidity in the range 75% to 90%, and refrigerant to air temperature differences of 5°C to 15°C. Heat transfer performance was based on a sensible air-side heat transfer coefficient which included the effect of frost. The rate of frost growth was found to be higher initially, until the thermal resistance of the frost layer lowered the temperature driving force. The rate of increase in air pressure drop, and decline in air velocity and sensible performance, was greater at higher relative humidities, higher air temperatures and larger temperature differences. It was observed that frost growth was greater in the first rows of the coil. At higher humidities performance peaked and declined sooner, than with lower humidities.

Gatchilov and Ivanova (1979) investigated frost structure and properties, and their influence on coil performance. Frost formation was seen to begin on the tubes, then move along the fins, starting at the base. This was only evident in the first 15 to 20 minutes, after which the frost thickness was approximately even, probably due to a reduced temperature gradient resulting from the initial frost formation. Frost structure and properties were observed to be different between the tubes and the fins, with the tubes having considerably smoother frost than the fins. Frost roughness decreased with time, and increased with higher relative humidity and increased air flow. Increased frost roughness lead to increased heat transfer coefficient, but also increased coil pressure drop. At high air velocity and humidity the highest roughness and thickness was observed on the first rows of the coil. Frost density was found to increase with time, increased relative humidity, and increased air flow. It was concluded that with wider fin spacing, frosted coil operation may be prolonged before the coil requires defrosting and that variable fin spacing performs better than constant

fin spacing.

Ivanova and Gatchilov (1983) conducted tests with air-on temperatures of -1°C to 2°C, relative humidities of 74% to 88%, temperature difference of 8°C to 10°C, and constant airflow for each trial (2 to 10 kg/m^2s). Increased humidity and air flow increased frost thickness for the same length of operation. After prolonged operation, the rate of increase in frost thickness reduced, as part of the water vapour in the air diffused in to the existing frost layer, to increase frost density.

Kondepudi and O'Neal (1987) reviewed the effects of frost growth on extended surface heat exchanger performance. This review was divided into the effect of frost on fin efficiency, overall heat transfer coefficient, pressure drop, and surface roughness. The conclusions reached were: Fin efficiency increases initially, and tends to a constant value; no verification of fin efficiency expressions had been presented; overall heat transfer coefficient has an initial rise, due to increased surface area and roughness of the frost, which is later offset by the insulation effects of the frost; overall heat transfer coefficient increases with relative humidity and airflow; heat exchangers with wider or variable fin spacing perform better under frosting conditions; pressure drop across the coil, and hence drop in air flow, was more influential than the insulation effect on heat transfer performance; surface roughness is difficult to predict, and can contribute to enhanced heat transfer in the initial stages of frost growth; roughness is affected by humidity and airflow. Kondepudi and O'Neal (1985) also noted that further experimental work on the exact effects of frost on coil performance is required, and that simple, yet accurate, correlations for overall heat transfer coefficient, based on coil geometry and environmental conditions would be useful.

Kondepudi and O'Neal (1989), performed trials in a tunnel type facility, on louvred finned tube heat exchangers, with fin densities from 14 to 18 fpi, relative humidity from 60 to 85%, face velocity between 0.6 m/s and 1.3 m/s, air temperature of 0°C, in a tunnel type facility. They quantified coil performance in terms of energy transfer coefficient, based on air enthalpy driving force. Experiments were conducted

at constant air flowrate. The energy transfer coefficient remaining approximately constant, until the later stages when it began to fall, which was attributed to the insulation effect of the frost. The energy transfer coefficient drop off was more rapid with increased frost growth, due to the higher insulation effect reducing the sensible heat transfer. Higher humidity, higher air flow, and high fin density gave higher energy transfer coefficients and increased rates of frost growth. Higher humidity leads to higher latent heat transfer, and more frost growth (attributed to higher mass transfer potential). Higher fin density gave more frost growth, as it provides more surface area for heat transfer, and higher localized air velocity between the fins. However as the free flow area decreases, the pressure drop across the coil increases, which results in faster performance decline. Factors which lead to increased frost growth, lead to increased pressure drop across the coil.

2.6 MODELS OF FROSTED COIL PERFORMANCE

2.6.1 Heat Transfer Only Models

A number of models, particularly those used in air conditioning applications, include the latent heat component in steady state models, but ignore the effect of the buildup of frost that occurs due to the latent heat transfer.

For air conditioning applications, where condensation rather than frosting occurs, a straight line law is usually used to describe the overall heat transfer (Stoecker and Jones, 1982; Stoecker, 1988). This approach assumes that the air transferring heat and mass to a wetted surface, follows a straight line on the psychrometric chart, from the air-on condition to the saturation line at the coil surface temperature. The change in temperature is proportional to the sensible heat transfer, while humidity difference is proportional to the latent heat component (Stoecker, 1988). This has important implications on the psychrometric chart, because the slope of the line representing the air conditions passing through the coil, is directly related to the sensible heat ratio (Cleland and Cleland, 1992). Using this approach, the *SHR* can be estimated from

a sensible heat transfer design, using:

$$SHR \approx \left[1 + \frac{\Delta h_{fg} \, (H_{on} - H_s)}{c_a \, (T_{on} - T_s)} \right]^{-1} \qquad (2.10)$$

The problem with this method is the estimation of the surface temperature, as it is not uniform across the coil surface. It is dependent on the relative size of the air and refrigerant side heat transfer resistances.

Stoecker and Jones (1982) showed that if the Lewis relationship between the sensible heat transfer coefficient and the mass transfer coefficient holds, the total heat load can be expressed in terms of sensible heat transfer coefficient and the enthalpy potential:

$$\phi_t = \frac{h_a A}{c_a} \, (\Delta h_m) \qquad (2.11)$$

where: h_a = convective heat transfer coefficient (W/m^2°C)

c_a = specific heat of moist air (J/kg°C)

Δh_m = mean enthalpy difference between the entering air and saturated air at the coil surface temperature (J/kg)

This may not be valid under frosting conditions, as the Lewis relationship may not be accurate.

Goldstein (1983) gave a mathematical analysis of a heat exchanger, operating under either dry or condensing conditions. The analysis is based on equating the refrigerant-side and air-side heat transfer capacities. The analysis did not allow for any frosting.

Sanders (1974), and Kondepudi and O'Neal (1989) used an enthalpy driving force rather than a temperature driving force, with an energy transfer coefficient in place of an overall heat transfer coefficient. The energy transfer coefficient was described

by:

$$U_h = \frac{c_a \phi_t}{(LMED)\ A} \tag{2.12}$$

where: $LMED$ = log mean enthalpy difference (J/kg)

U_h = energy transfer coefficient (W/m^2°C)

The difficulty with this approach is that the LMED requires the enthalpies of both air and refrigerant. In practice combining these two is somewhat difficult, as different datums are used. This is overcome by assuming the refrigerant enthalpy to be that of saturated air at the refrigerant temperature. Thus the LMED is defined as:

$$LMED = \frac{(h_{a\,on} - h_{r\,out}) - (h_{a\,off} - h_{r\,in})}{\ln\left[\dfrac{h_{a\,on} - h_{r\,out}}{h_{a\,off} - h_{r\,in}}\right]} \tag{2.13}$$

where: $h_{a\,on}$ = enthalpy of air entering coil (J/kg)

$h_{a\,off}$ = enthalpy of air leaving coil (J/kg)

$h_{r\,in}$ = enthalpy of refrigerant entering coil (J/kg)

$h_{r\,out}$ = enthalpy of refrigerant leaving coil (J/kg)

This is similar to Equation (2.11), but is not limited by the determination of U_h through the Lewis relationship.

Cornelius (1991) and Cleland and Cleland (1992) all ignored the change in coil performance as frosting occured, but gave equations to predict the *T:S* ratio (or *SHR*), from air-on and refrigerant evaporation temperature. In this way sensible heat transfer rates could be adjusted to take account of the latent heat transfer component. No experimental validation of the equations was reported.

2.6.2 Types of Frost Models

Many researchers have observed that frost properties and their effect on heat transfer performance changes significantly with coil operating conditions. Smith (1989) proposed the concept of "unfavourable" frost formation to describe why differences in frost properties are observed. It was suggested that unfavourable frost formation occurs when the line representing the temperature and humidity of the air passing through the coil, crosses the saturation line of the psychrometric chart (Figure 2.1). Under these conditions (high RH_{on}, low *SHR*, high temperature difference), it is suggested that airborne ice-crystal precipitation will occur, and the frost will be of particularly low density. This would both insulate the coil surface and reduce airflow at a much greater rate than under favourable frost formation conditions.

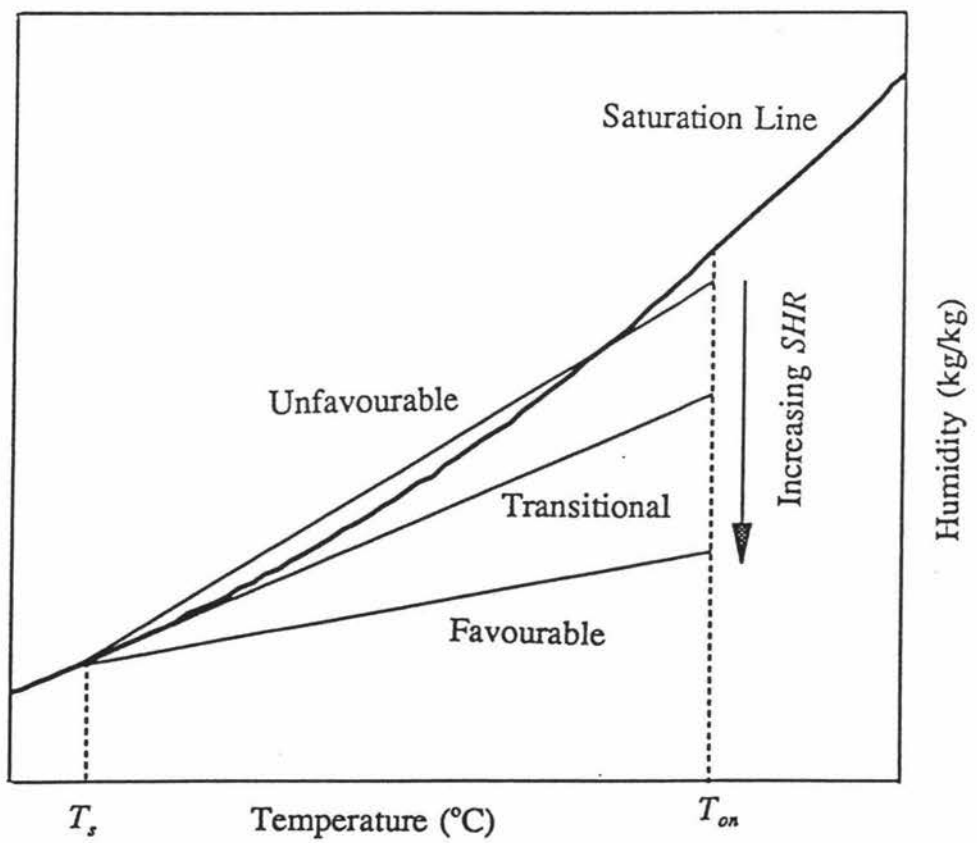

Figure 2.1 Psychrometric chart showing concept of favourable and unfavourable frost formation for air cooling coils.

2.6.3 Overall Performance Models

Hosoda and Uzuhashi (1967) developed a number of empirical equations for frost properties and coil performance, based on their experimental results for flat plates and coils (Section 2.5.2). They gave relationships for frost density, thermal conductivity, the surface heat transfer coefficient of the frost, an overall heat transfer coefficient of frost on a finned coil, and the pressure drop for the coil. The overall heat transfer coefficient was determined from the maximum air velocity between the fins. They found overall heat transfer performance with frost formation to be greater than dry coil performance, until a frost thickness of approximately 2 mm had formed.

Sanders (1974) performed an analytical study of finned tube heat exchangers under frosting conditions. The study began with a fundamental investigation into frost formation and growth, using the enthalpy potential and a modified Lewis relationship. A relationship for frosted fin efficiency was developed, that showed fin efficiency to increase with increasing frost thickness. The coil was divided into several "transfer elements", which were assumed to be homogeneous in nature. The heat transfer to an "element" was calculated, using dry heat transfer coefficients for the air-to-fin, and various geometric factors which take into account the changing shape of the coil as frost forms. Equations from the resulting integration over the entire coil, for two different coil geometries, were used to predict capacity against time for various operating conditions. These showed cooling capacity and air flow to fall as frost accumulates on the coil. The model was not designed to be extremely accurate itself, but rather to show trends under various coil configurations and environmental conditions. Sanders notes that for greater model accuracy, more accurate surface heat transfer coefficients and frost properties are required.

Kondepudi and O'Neal (1993a, 1993b) developed a model to predict the performance of finned tube heat exchangers under frosting conditions. The quasi-steady state model was divided into two components, prediction of the frost layer deposition and properties, and the heat exchanger performance. The frost deposition rate was

determined from the loss of air humidity. Water vapour was assumed to increase both frost height and density. Frost porosity was estimated, from which an empirical method was used to calculate the diffusion coefficient of vapour in frost. Frost density and thermal conductivity were then calculated. An overall energy transfer coefficient was used to measure the heat exchanger performance, as in Equation (2.12). A measure of the frost layer heat transfer was incorporated in the air-side heat transfer coefficient. The refrigerant enthalpy was approximated by the enthalpy of saturated air at the refrigerant temperature. The air-side heat transfer coefficient was estimated by the Gray and Webb (1986) expression for flat finned coils.

The model was used to show trends of various parameters of frosted coil operation, such as frost growth, energy transfer coefficient, and pressure drop, against time. Experimental data was generally within 15-20% of predicted values, and showed similar trends to that reported elsewhere in the literature. Discrepancies were attributed to errors in air-side heat transfer coefficient prediction and frost properties estimations.

3 RESEARCH OBJECTIVES

Whilst frosting on coils is influential on performance, there is comparatively little information available on the performance of finned tube heat exchangers under frosting conditions (O'Neal and Tree, 1985). A substantial amount of work has been done on frost properties and growth, but mainly for simpler geometries such as tubes, annuli, and plates. This paucity of information has been attributed to complex geometries and the large number of variables that can affect performance, compounded with extremely complex frosting models (Kondepudi and O'Neal, 1987).

The work on frosting of finned tube heat exchangers has been mainly experimental in nature. Most experimental investigations into frosted cooling coil performance have been performed with constant air flowrate, and lower relative humidities (high sensible heat ratio). These conditions are not representative of the conditions under which coils are usually operated in industry. In many refrigeration applications fan speed is uncontrolled, and air flowrate is determined by the pressure drops in the system. As frosting occurs the extra pressure drop results in a decline in flowrate. Additionally, in many applications, coils are located in areas that can experience particularly low local *SHR*, e.g. near doors. Kondepudi and O'Neal (1993a, 1993b) give one of the only comprehensive model of a finned tube heat exchanger under frosting conditions, showing performance trends, as frost grows on the coil surface.

According to the theory of favourable and unfavourable frost formation proposed by Smith (1989), unfavourable frost would form when the line representing the air conditions on a psychrometric chart, crosses the saturation line. Under these conditions (high RH_{on}, low *SHR*, high *TD*), it is suggested that airborne ice-crystal precipitation will occur, and the frost will be of particularly low density. This would both insulate the coil surface and reduce airflow at a much greater rate than under favourable conditions. Much of the previous experimental work appears to have been performed within the favourable frost formation region, avoiding such problems.

The objectives of this research were to:

(a) Measure frosted cooling coil performance under conditions similar to those encountered in industry, with declining air velocity, and a range of humidities and sensible heat ratios (including those potentially leading to unfavourable frost formation).

(b) Identify and quantify the effect of parameters affecting frosted coil performance under such conditions.

(c) Assess the validity of Smith's theory of favourable and unfavourable frost formation.

(d) If appropriate, test Smith's theory for the prediction of a transition condition between favourable and unfavourable frost formation.

4 EXPERIMENTAL DATA COLLECTION

4.1 COIL PERFORMANCE TEST FACILITY

4.1.1 General Description

Coil heat transfer performance was measured in a calorimeter style test facility, similar to that suggested in the ASHRAE and Dutch standards (ASHRAE Standard 25-77, Netherlands Standard NEN 1876). The major difference was that the facility was designed to operate in a manner more consistent with industrial operation of cooling coils. This involved the heat load being held constant, whilst the refrigerant temperature was modulated to maintain a constant air-on temperature. Coil performance was quantified by energy balances as in the standards (ASHRAE Standard 25-77, Netherlands Standard NEN 1876). The test facility allowed both heat input and removal rates to be accurately measured and controlled. A schematic diagram of the test facility is shown in Figure 4.1.

The facility was 2.4 m high, 2.7 m wide, and 4.2 m long, constructed of 150 mm polystyrene sandwich panel. The test coil was centrally mounted, suspended from the ceiling. The air-on and air-off sides of the facility were separated by a wooden divider. A dry heat addition system (dry heater) and a wet heat addition system (humidifier) were located in a 1.27 m by 0.76 m air transfer tunnel passing through the divider.

The dry heater consisted of a bank of nine electrical resistance heating elements ranging from 0.5 to 2.0 kW in size, of which any combination could be used. The humidifier consists of an insulated, electrically heated, boiling water bath, located under the facility. A sparge pipe connected the water bath to the facility, and entered the facility upstream of the dry heaters. A butterfly valve enabled the generated steam to either enter the facility, or be vented to ambient. Power input to the humidifier could be varied, to alter the steam entry rate. Humidifier water level was kept constant, by use of gravity feed from an external water tank.

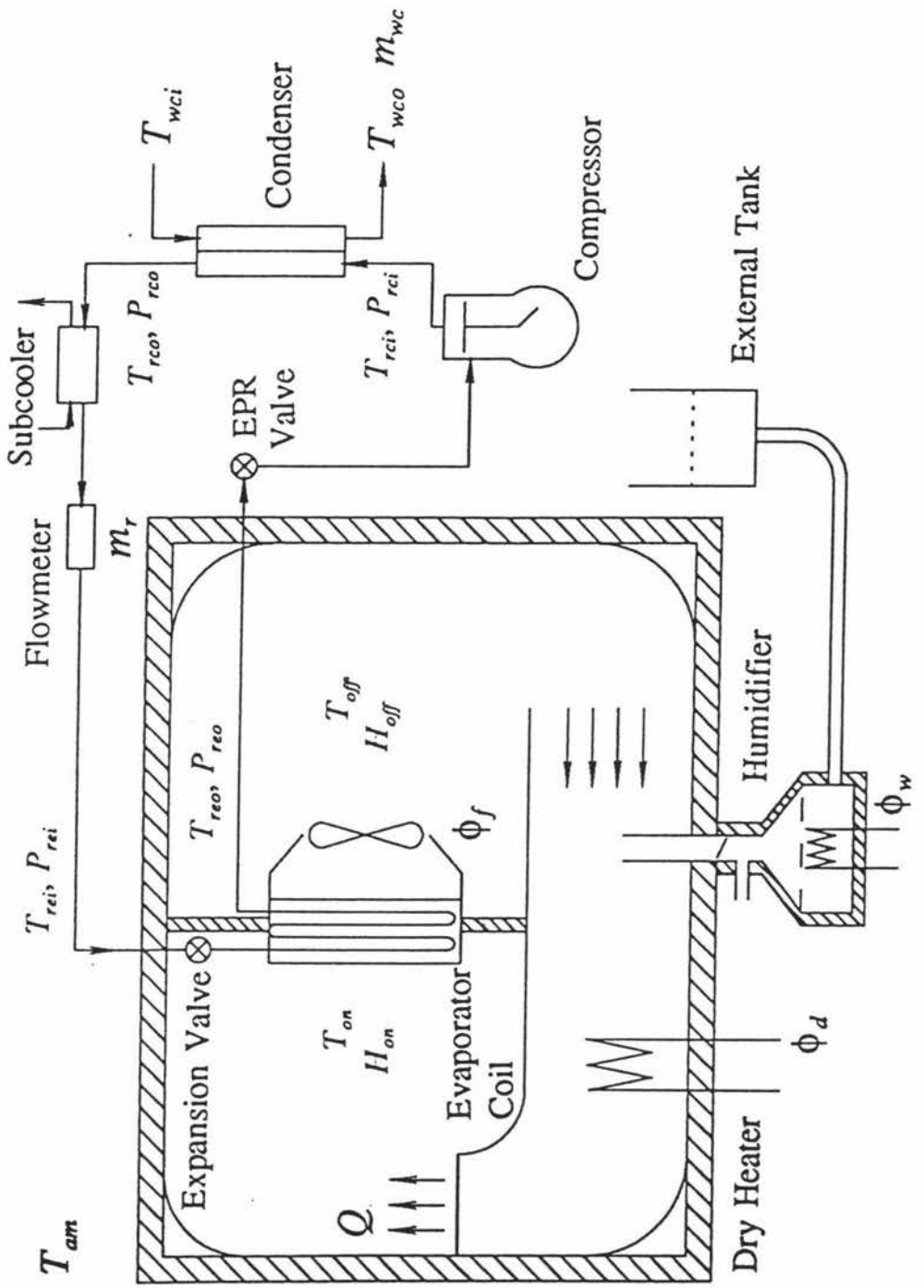

Figure 4.1 Schematic diagram of the coil performance test facility.

The coil was connected to a standard single stage refrigeration plant, with a water cooled condenser/receiver, operating with refrigerant HCFC-22. The nominal capacity of the plant was approximately 15 kW at -6°C suction temperature, and 30°C discharge cooling temperature. The compressor was operated continuously. A Danfoss KVQ electronic evaporation pressure regulating (EPR) valve controlled both the capacity of the compressor, and the coil air-on temperature to the set point to the desired set-point. Liquid refrigerant feed to the coil was controlled by a thermostatic expansion valve. The expansion valve was adjusted to the minimum superheat that gave stable operation.

4.1.2 Coil Description

The test coil used was a typical commercially available direct expansion model, with the following characteristics:

Coil Block Dimensions	1.450 m long, 0.685 m high, 0.131 m deep.
Tubes	5/8" copper (14.4 mm ID, 16.2 mm OD), triangular pitch, 21.9 mm between centres, 18 rows high, 4 rows deep.
Circuiting	6 circuits of 12 tubes, counter-current to air flow.
Fins	aluminium, wavy shaped, 0.254 mm thick, 157 fins/metre (4 fpi).
Fans	2 induced draught Ziel-Abegg SC050.VDQ.4F.5 (operating on low speed).
Expansion Valve	Danfoss TEX2, orifice number 4.

For all experimental work except five trials (trial numbers 3, 4, 9, 10, and 11) the coil did not have a suction line heat exchanger. For these trials, a suction line heat exchanger was added, with the expansion valve bulb placed approximately 1.5 m down-stream of the heat exchanger to maintain stable operation. The heat exchanger was added for performance testing purposes, and resulted in a marginal drop in suction temperature (less than 5%) compared to similar trials without the heat

exchanger.

4.1.3 Measurement Systems

The facility was extensively monitored via a computer based electronic data logging system. Air temperature, humidity, and flowrate; refrigerant temperature, pressure, and flowrate; heat inputs to the dry heaters, humidifier, and fans; and condenser water flowrates and temperatures were all measured.

Air, Water, and Refrigerant Temperatures

Air, water, and refrigerant temperature measurement was accomplished with a combination of copper-constantan (type T) thermocouples (with an ice-point reference junction) and PT100 resistance probes. All temperature sensors were covered in shiny aluminium foil to minimise radiation effects. Air-on and air-off temperatures were based on the average of a grid of 6 sensors on each side of the coil, and 3 randomly placed in each section. Air-off temperature was measured on the exit side of the fans. As shown in Figure 4.1, refrigerant temperature measurement locations included: condenser inlet, T_{rci}; condenser outlet, T_{rco}; immediately before the expansion valve, T_{rvi}; and on three circuits of the coil, at the inlet, T_{rei}, circuit mid point, T_{rem}, and coil outlet before the EPR valve, where T_{reo} was taken. Probes measuring refrigerant temperature were attached to the appropriate pipe with heat sink material between the sensor and the pipe. The pipe and sensor were then insulated from the ambient conditions with either 25mm foam insulation or a cork based insulation tape. Outside ambient temperature (T_{am}) and condenser water inlet and outlet temperatures (T_{wci} and T_{wco}) were also measured. All temperature sensors were calibrated using an ice-point, with accuracy estimated to be ±0.25°C.

Air Humidity

Air-on dewpoint temperature ($T_{dp\,on}$) was measured with a Michell Series 3000 cooled mirror dewpoint meter. The dewpoint meter was inherently accurate, being based on

temperature measurement, and factory calibrated to a UK standard. The meter self-calibrated at start-up and every 2 hours, to compensate for any dust or dirt on the mirror. The stated accuracy for the dewpoint meter was ±0.3°C. The air-off humidity (H_{off}) was measured with two Vaisala HMP 113Y capacitance type sensors, accurate to ±2% below 80% relative humidity and ±3% above 80% relative humidity, when calibrated against salt solutions. The Vaisala probes were calibrated every 4 to 6 weeks against reference saturated salt solutions. The salt solutions used were NaCl, 75.45 ±0.14% *RH* at 20°C, and KNO_3, 94.62 ±0.66% *RH* at 20°C (Greenspan, 1976).

Refrigerant Pressures

Refrigerant pressures throughout the refrigeration system, were measured with Danfoss EMP2 pressure transducers. The six measurement locations, shown in Figure 4.1, were: the condenser outlet, P_{rco}; immediately before the expansion valve, P_{rvi}; between the expansion valve and the distributer, P_{rvo}; the coil inlet at the beginning of a circuit, P_{rei}; coil outlet before the back pressure valve, P_{reo}; and after the back pressure valve, P_{rvo}. In addition, the compressor discharge pressure was measured manually from the gauge at the compressor. The pressure sensor between the expansion valve and the distributer became redundant, for those trials with the suction line heat exchanger added. The position of the expansion valve was altered to accommodate the addition of the heat exchanger. Pressures on the low pressure side of the refrigerant circuit were measured with transducers with a -1 to 5 bar range, while on the high pressure side 0 to 16 bar transducers were used. Pressure accuracy was ±1% of full scale output (±0.06 bar for low pressure, and ±0.16 bar for the high pressure side). Factory calibration was performed prior to commissioning. Comparison of readings with the system at steady state during off periods, showed disagreement between the transducers of less than ±0.1 bar.

Refrigerant Flowrate

Refrigerant mass flow rate was measured with a Danfoss MASSFLO flowmeter, type

MASS 1100. This was installed in the liquid line between the condenser and the expansion valve. A small water cooled refrigerant subcooler was located before the mass flowmeter to ensured flashing of the liquid refrigerant in the flow meter did not occur. The output of the flowmeter was zeroed when refrigerant was bypassing the meter (i.e. no flow through the meter). Refrigerant flow measurement was only started (by closing the bypass) once operation of the refrigeration system was stable. Accuracy of the flowmeter was specified at ±1% of the measured value. Calibration of the meter was also checked with a heat balance over the condenser (Section 5.4).

Power Inputs

The line voltage (V), and the current (I) drawn by each of the fans, dry heater and humidifier were measured. The line voltage was measured using a line voltage transformer. The humidifier and fan current was measured using a Radio Spares current transducer, using Hall effect IC and giving an RMS output. The dry heating element current measurement was made with a wire current shunt circuit, built by the Department of Process and Environmental Technology at Massey University. Due to the inductive nature of the fan load, a single measurement of the phase angle difference between current and voltage (PF) was also taken. This test measurement was made with a Dranetz 8000, from GTS Nilsens instruments.

Data Logging

Most of the above sensors had electronic outputs and were monitored and logged on a PC based data logging system. All the PT 100, current and voltage sensors, humidity probes, and refrigerant massflow signals were connected to an Analog Devices 5B02 analog board. Appropriate 5B Analog Devices modules converted incoming signals to a -5 to +5 output voltage. This voltage was then converted on an RTI-820 analog-to-digital conversion board. The output from this was then monitored and logged using the FIX software package (Intellution Inc, 1988). The thermocouples were connected to an Analog Devices STB-TC board, before going to the RTI board with the other signals. Data were logged at 6 second intervals.

Air Flowrate

A thin wire mesh screen (mesh number 16), covered the discharge end of the air transfer tunnel to improve uniformity of air velocity distribution for air flowrate measurement. At the start of each trial, an initial air flowrate measurement, Q_0, was taken as the average of 28 air velocity measurements taken in a regular 7 by 4 grid pattern over the mesh screen at the end of the air transfer tunnel, at the start of each trial. Changes in a single representative air velocity measurement, v, taken at a point above the mesh were used to scale the initial air flowrate measurement, Q_0, to give the instantaneous flowrate (Q). This system meant that the air velocity could be measured without entering, or disturbing, the operation of the test facility after frost formation had commenced. All velocities were measured using a Testovent 4000 vane anemometer, accurate to ±0.1 m/s, in the range of 0.4 to 40 m/s. Calibration was also checked against a hot wire anemometer, known to be calibrated to ±0.1 m/s, in the range of 0 to 5 m/s. In practice, the accuracy of the measured air flowrate is somewhat less that the accuracy of these instruments, due to non-uniformity of the air flow, with respect to both time and position. The accuracy was assessed as being of the order of ±20% at the worst case conditions (high relative humidity, low *SHR*, and low air velocities).

Water Flowrate

Condenser water flowrate was measured manually, by timed mass collection from the condenser water outlet. The mass of water in the humidifier feed tank, was also periodically weighed to give a measure of the rate of water input to the test facility.

4.2 EXPERIMENTAL PROCEDURE

4.2.1 Initial Setup and Dry Performance

Before each trial began, the humidifier was bought up to temperature with the humidifier steam being vented to ambient. The facility was started and pulled down to the set-point air-on temperature, without any heat addition. The initial air flowrate measurement, Q_0, was then made.

The dry heaters were then started. Once conditions had stabilised, an initial coil performance measurement was taken, using data averaged over a ten minute period, with a dry heater input of 7.2 kW. Humidifier steam was still being vented to ambient. This initial dry performance was used as a reference for the frosted coil performance.

4.2.2 Frosted Coil Performance

After the initial dry coil performance measurement, the electrical inputs to the dry heater and humidifier were then reset to give the desired sensible heat ratio, *SHR*, and total heat load, ϕ_t, taking ingress and fan heat inputs into account. Steam addition was initiated by opening the butterfly valve in the sparge pipe from the humidifier, and sealing the vent to ambient. Throughout each trial manual measurements of the compressor discharge, humidifier feed tank mass, condenser water flow, and relative air velocity were taken, at approximately 10 to 20 minute intervals. Air flowrate was calculated using the initial flowrate, Q_0, scaled against the relative velocity measurements, v/v_0.

At regular intervals the instantaneous coil performance was measured, using data averaged over a three minute period. During each trial between six and ten such measurements were taken, every 20 to 40 minutes. A trial concluded once a predetermined amount of water had been added to the facility, or the air flowrate had declined to less than 40% of the initial value, Q_0.

4.3 EXPERIMENTAL TRIALS

A number of experimental trials were required to develop appropriate experimental procedures. Sixteen trials were performed with dry heat addition only, to develop and test the measurement systems and testing procedures. A further 40 dry only heat addition trials were conducted to test the coil performance over a range of heat loads and temperatures. The results of these enabled a correlation for the refrigerant -side heat transfer coefficient to be developed. The data was also required by the sponsoring organisations but were not directly relevant to this frosting study, and are therefore not reported.

Further trials were required to develop the control and measurement systems for the moisture addition system and experimental protocol for wet heat addition trials. A total of 30 such trials were conducted, over a range of temperatures. Once the procedure and measurement system hade been refined sufficiently that collection of reliable data was possible, a full set of 16 long term trials with frosting were performed. This included replicate runs to judge repeatability. A summary of the test conditions used in these later trials are shown in Table 4.1. All of these trials were performed with a nominal air-on temperature, T_{on}, setpoint of 0°C. Heat inputs were held constant so that heat loads were between 6.5 kW and 10.0 kW (including ingress and fan power), and the *SHR* was between 0.54 and 0.84.

For trials 7, 12, 14, 15, and 16, after the period of constant low *SHR*, the steam addition was terminated, and the facility was operated for a further 50-60 minutes with only the dry heater operating. Instantaneous coil performance was then remeasured.

Five additional trials were performed with a nominal air-on temperature set point of -20°C, but encountered serious technical difficulties. Frosting and snow formation inside the test room occurred (mainly on the mesh at the end of the air transfer tunnel). This resulted in air flow measurement being extremely inaccurate, which lead to inaccurate mass balances across the coil. Solutions to these problems would

have required further significant capital investment in the test facility, which was beyond the scope of this study. Thus a detailed analysis of frosting temperatures below 0°C was not attempted.

4.3.1 Experimental Accuracy

During any trial, T_{on} varied by less than ±0.2°C from its mean, and relative humidities, RH_{on} and RH_{off}, were both stable, varying by less than ±2%. Refrigerant superheat was typically 5-7°C at the start of a trial, and increased slightly as the trial progressed. The initial coil performance, UA_0, varied by less than ±10% between trials.

Table 4.1 Experimental conditions for coil performance trials under frosting conditions

Trial	T_{on} (°C)	RH_{on} (%)	SHR	ϕ_t (kW)	Trial	T_{on} (°C)	RH_{on} (%)	SHR	ϕ_t (kW)
1	-0.2	68	0.84	8.1	9	-0.6	78	0.70	9.2
2	-0.4	68	0.83	7.9	10	-0.4	81	0.70	9.8
3	-1.6	72	0.78	8.5	11	-1.4	87	0.70	8.6
4	-0.8	83	0.71	6.7	12	-0.7	89	0.63	7.9
5	-1.6	82	0.71	6.5	13	-1.8	87	0.62	7.6
6	-0.3	82	0.71	6.5	14	-0.1	87	0.58	8.3
7	0.0	76	0.70	9.8	15	0.1	93	0.54	9.3
8	0.2	77	0.70	9.9	16	0.2	93	0.54	9.3

5 DATA ANALYSIS

5.1 DATA ACQUISITION AND VALIDATION

Data for each period of interest in a trial was logged using the FIX software, then transferred to a spreadsheet for analysis. Except for the initial dry performance, which was averaged over 10 minutes, each estimate of performance was based on the data averaged over a 3 minute period. For each of the logged data variables, the mean, minimum, maximum values, and standard deviation were calculated. These were individually checked, and any anomalies were investigated. In some cases not all the data were successfully down-loaded, or extreme outlier's were recorded. If considered justifiable, such outlying points were deleted from the data set. A detailed description of the calculations performed by the spreadsheet follow. A full example of the output for trial 2 after 346 minutes is given in **Appendix** A.2.

5.2 QUANTIFICATION OF COIL PERFORMANCE

In each trial, the total heat input to the facility, and sensible heat ratio, were held constant. The refrigerant evaporation temperature was automatically modulated by the evaporator back pressure valve, to maintain the desired air-on temperature, as the coil performance deteriorated with frosting. A parameter to measure the instantaneous coil performance was required that changed with frost accumulation, was independent of air to refrigerant temperature difference, and was equally applicable to trials of different sensible heat ratios, and therefore air-on relative humidity values, and total heat loads.

The parameter chosen to best meet these criteria was the coil's sensible capacity rating, *UA*:

$$UA = \frac{\phi_s}{TD_m} \tag{5.1}$$

$$TD_m = \frac{(T_{on} - T_{off})}{\ln\left[\frac{(T_{on} - T_{re})}{(T_{off} - T_{re})}\right]} \tag{5.2}$$

where:

ϕ_s = sensible heat input (W)

T_{on} = air-on temperature (°C)

T_{off} = air-off temperature (°C)

T_{re} = refrigerant evaporation temperature (°C)

TD_m = mean temperature difference (°C)

UA = instantaneous coil sensible capacity rating (W/°C)

As discussed in Chapter 2, a number of alternative performance definitions are available, but not all were relevant to the way in which the trial were performed. For example, the Dutch coil testing standard used an average performance until frost reduces performance to 85% of the initial performance, and also considers defrost. The overall enthalpy performance coefficient, defined in terms of enthalpy differences, used by Kondepudi and O'Neal (1989), requires either an estimate of coil surface temperature, or assumes that the saturated air enthalpy at the refrigerant temperature can be used. The use of UA is consistent with industrial practice, where generally only the sensible heat performance is considered in detail. Thus, use of the enthalpy coefficient could not be justified, unless use of the simpler sensible heat rating proved unsatisfactory.

Refrigerant-side pressure drop and superheat effects on TD_m were ignored, which is consistent with normal commercial coil rating practice. Hence, T_{re} was taken as the saturated evaporation temperature corresponding to the coil exit refrigerant pressure, P_{reo}.

Due to the fans being an integral part of the evaporator, the measured air-off

temperature, $T_{off\ meas}$, was taken after the fans. Measured values were adjusted to allow for heating of the air, as the air passed through the fans, using:

$$T_{off} = T_{off\ meas} - \frac{\phi_f\ 0.5}{Q\ \rho_a\ c_a} \tag{5.3}$$

where:
- ϕ_f = total fan heat input (W)
- Q = air flowrate (m^3/s)
- ρ_a = air density (kg/m^3)
- c_a = specific heat capacity of air (J/kg °C)
- $T_{off\ meas}$ = measured air-off temperature (°C)

This assumes that the air temperature change across the fans corresponds to an arbitrarily assessed, 50% instantaneous conversion of the fan energy input, to heat.

To allow comparison of performance deterioration with different sensible heat loads and fan speeds, the *UA* values were normalised on a 0 to 1 scale, by dividing the instantaneous *UA* value by the *UA* measured for the dry heat only period, at the start of each trial (UA_0). The change in air flowrate through the coil was normalised in a similar manner:

$$\frac{UA}{UA_0} \quad \text{and} \quad \frac{Q}{Q_0} \tag{5.4}$$

where:
- UA_0 = coil sensible capacity rating at the start of a trial (W/°C)
- Q_0 = initial air flow rate through the coil (m^3/s)

For trial 16 the initial heat load for the dry only reference was not 7.2 kW, as in the other trials. Therefore the mean UA_0 value for all the other trials was used as the UA_0 for trial 16, so that it could be compared to the other trials on the same basis.

5.3 SENSIBLE HEAT LOAD

A value of ϕ_s is required to estimate *UA* in Equation (5.1). Two alternative estimates were considered: based on the change in air temperature through the coil, or based on the sensible heat inputs entering the test facility. The sensible heat loss from the air passing through the coil, is given by:

$$\phi_{as} = Q\ \rho_a\ c_a\ (T_{on} - T_{off}) \tag{5.5}$$

The sensible heat inputs to the facility are given by:

$$\phi_{is} = \phi_d + \phi_f + \phi_{hs} + \alpha\ \phi_{am} \tag{5.6}$$

where:
- ϕ_{as} = air -side sensible heat load (W)
- ϕ_{is} = sensible only heat inputs (W)
- ϕ_d = dry heater input (W)
- ϕ_f = fan heat input (W)
- ϕ_{hs} = sensible humidifier heat input (W)
- ϕ_{am} = heat ingress from ambient (W)
- α = fraction of ingress load that is sensible

It was assumed that ϕ_d was sensible only, and was taken as the electrical power supplied to the heater elements:

$$\phi_d = I_d\ V_d \tag{5.7}$$

where:
- I_d = current drawn by the dry heaters (A)
- V_d = dry heater power supply voltage (V)

ϕ_f was taken as the total power input to the fans, being sensible only, and included a power factor correction, due to the inductive nature of the fans:

$$\phi_f = I_f\ V_f\ PF_f \tag{5.8}$$

where: I_f = current drawn by the fans (A)

V_f = fan supply voltage (V)

PF = power factor

PF was measured to be 0.90.

ϕ_{hs} is the sensible component of the humidifier heat addition. Although the humidifier contributes mainly a latent load, a small fraction is sensible due to the cooling of the injected steam from the humidifier water temperature, T_{wh}, to the coil air-on temperature, T_{on}. Therefore:

$$\phi_{hs} = m_{wh}\, c_{wv}\, (T_{wh} - T_{on}) \tag{5.9}$$

where: m_{wh} = mass flowrate of water vapour into the test facility (kg/s)

c_{wv} = specific heat capacity of water vapour (J/kg °C)

T_{wh} = humidifier water temperature (°C)

The rate of water vapour addition to the test facility, by the humidifier, m_{wh}, was estimated from the electrical power supplied to the humidifier, subtracting heat losses to ambient, and energy required to heat the feed water to the humidifier temperature;

$$m_{wh} = \frac{I_h\, V_h - k_{loss}(T_{wh} - T_{am})}{\Delta h_{fg} + c_{wh}\, (T_{wh} - T_{am})} \tag{5.10}$$

where: c_{wh} = specific heat of water in humidifier (J/kg °C)

Δh_{fg} = latent heat of evaporation (J/kg)

I_h = current drawn by the humidifier (A)

k_{loss} = heat loss factor from humidifier (W/°C)

T_{am} = ambient air temperature (°C)

V_h = humidifier supply voltage (V)

This relationship assumes that heat transfer by conduction through the sparge pipe connecting the humidifier to the facility is negligible, that the enthalpy of superheated

steam is the same as the enthalpy of saturated steam at the same temperature (Stoecker and Jones, 1982), and that the sensible heat effects of frost on the coil are negligible. The heat loss factor, k_{loss}, was estimated to be 2.5 (W/°C).

ϕ_{am} is the heat ingress from the ambient air, through the insulated walls, and through the door seals. It was estimated from measurements of T_{am}, T_{on}, and T_{off}, using:

$$\phi_{am} = 0.22\ E\ [\ A_{am\ on}\ (T_{am} - T_{on}) + A_{am\ off}\ (T_{am} - T_{off})] \qquad (5.11)$$

where:
$A_{am\ on}$ = air-on side room surface area (m^2)
$A_{am\ off}$ = air-off side room surface area (m^2)
E = insulation effectiveness

For this calculation the facility was divided into two halves. The heat flow was then based on the temperature difference between ambient and either the air-on or air-off temperature. It was assumed that the insulation was the controlling heat transfer resistance, which had an estimated thermal conductivity of 0.033 W/m °C. An insulation effectiveness factor, E, to allow for leaky seals, air leakage, and air penetrations through the insulation, was included. E was estimated to be 1.75, which gave good heat balances for the earlier trials, under dry heat load conditions.

The fraction of ambient ingress load that is sensible, α, was assumed to be 0.9; accurate data was not essential, as sensitivity of results to α was low.

Of the two alternatives, ϕ_{is} was chosen as the best estimate of ϕ_s, because of the large uncertainty associated with measuring air flowrate, Q, and the uncertainty in accurately measuring the change in air temperature across the coil.

5.4 SENSIBLE HEAT RATIO AND TOTAL HEAT LOAD

The sensible heat ratio, *SHR*, is a key parameter in the analysis of coil performance. It is defined as:

$$SHR = \frac{\phi_s}{\phi_t} \tag{5.12}$$

where: ϕ_t = total heat load (W)

SHR = sensible heat ratio

Estimation of *SHR* required quantification of the total heat load. ϕ_t could be estimated in three ways; from a refrigerant side heat balance, from measurement of total heat additions to the test facility, or from the change in air temperature and humidity through the coil.

Refrigerant Side Heat Balance

The refrigerant side energy balance across the coil was based on the enthalpy change to the refrigerant, between the coil inlet and outlet:

$$\phi_{rt} = m_r (h_{reo} - h_{rei}) \tag{5.13}$$

where: ϕ_{rt} = refrigerant-side total heat flow (W)

h_{reo} = refrigerant enthalpy at coil outlet (J/kg)

h_{rei} = refrigerant enthalpy at coil inlet (J/kg)

m_r = refrigerant mass flowrate (kg/s)

Refrigerant enthalpies, h_{reo} and h_{rei}, were determined from measurements of T_{reo} and P_{reo}, and T_{rei} and P_{rei}, respectively, using the relationships given in Section 5.6. The values of h_{rei} and h_{reo} are likely to be accurate, as they not particularly sensitive to pressure measurement imprecision, and temperature measurements were considered accurate.

The measurement of refrigerant flowrate, m_r, was proven accurate through a heat balance over the refrigeration system at the condenser, between the cooling water and the refrigerant. The heat gained by the water in the condenser was calculated by:

$$\phi_{wc} = m_{wc}\, c_w\, (T_{wco} - T_{wci}) \qquad (5.14)$$

where:

ϕ_{wc} = condenser water heat flow (W)

c_w = specific heat capacity of water (J/kg °C)

m_{wc} = condenser water flowrate (kg/s)

T_{wco} = condenser water outlet temperature (°C)

T_{wci} = condenser water inlet temperature (°C)

c_w was taken from steam tables (Cooper and Le Fevre, 1986), for the water temperature range in the condenser. The water flowrate was calculated from an average of 3-5 timed samples, collected at the condenser outlet. The more variation in the mass of water collected, the more samples were taken, until at least three readings agreed within 5%.

The heat lost from the refrigerant passing through the condenser was calculated from the change in enthalpy of the refrigerant, as it passed through the condenser;

$$\phi_{rc} = m_r\, (h_{rci} - h_{rco}) \qquad (5.15)$$

where:

ϕ_{rc} = refrigerant-side condenser heat flow (W)

h_{rci} = refrigerant enthalpy at condenser inlet (J/kg)

h_{rco} = refrigerant enthalpy at condenser outlet (J/kg)

The refrigerant enthalpies were estimated from the curve fit equations, as specified in Section 5.6, based on measurements of refrigerant pressure and temperature at the condenser inlet and outlet. Heat losses from the condenser to ambient were estimated using a well known relationship for natural convection given by Coulson and Richardson (1977). These losses were found to be insignificant and were not included in the heat balance.

The difference between ϕ_{wc} and ϕ_{rc} was less than 5% in all cases, indicating that m_r measurement was probably accurate to better than ±3%. Thus Equation (5.13) was

considered accurate overall.

Heat Inputs to the Test Facility

The second method of calculating ϕ_t was by summing the rates of heat addition to the test facility:

$$\phi_{it} = \phi_h + \phi_d + \phi_f + \phi_{am} \tag{5.16}$$

where: ϕ_{it} = total input heat load (W)

ϕ_h = net heat input to the humidifier (W)

ϕ_h was taken as the electrical load on the humidifier, adjusted for losses to ambient:

$$\phi_h = I_h V_h - k_{loss} (T_{wh} - T_{am}) \tag{5.17}$$

Other load components have already been discussed.

Air-Side Heat Balance

Thirdly, ϕ_t was calculated from the changes in air temperature and humidity, as the air passes through the coil:

$$\phi_{at} \approx Q_a \rho_a c_a (T_{on} - T_{off}) + Q_a \rho_a \Delta h_{ig} (H_{on} - H_{off}) \tag{5.18}$$

where: Δh_{ig} = latent heat of water from vapour to solid (J/kg)

H_{on} = air-on absolute humidity (kg/kg)

H_{off} = air-off absolute humidity (kg/kg)

H_{on} and H_{off} were estimated from measurements of T_{on}, T_{off}, air-on dew point, $T_{dp\ on}$, and RH_{off}, as shown in Section 5.7.

The refrigerant side heat balance, ϕ_r, was used as the best estimate of ϕ_t, as it was

inherently the most accurate. The difference between ϕ_{rt} and ϕ_{it} was always less than 10%. ϕ_{at} had poorer agreement with the other two estimates of ϕ_t, especially at lower *SHR*. This was attributed to measurement imprecision in Q and H_{off}, in particular.

5.5 FROST ACCUMULATION

A measure of frost accumulation on the coil was required for comparison of the performance decline of the coil. The frost accumulated on the coil was taken as the amount of water added to the facility, assuming that all deposited water was on the coil surface. Two estimates were possible. Firstly, that based on the electrical heat input to the humidifier, subtracting losses and sensible heat effects, as given by Equation (5.10). Secondly, by the measured amount of water added from the external humidifier feed tank. The water addition rate from the external feed tank was calculated by averaging the change in mass of humidifier feed tank over the time interval between measurements.

These alternate estimates agreed within ±5% for all trials. An example of the cumulative water addition given by both methods is shown in Figure 5.1. For some trials the cumulative amounts of water supplied by the two methods were significantly offset, but had the same slope. The reason for this offset was discovered to be overfilling of the humidifier at the start of the trial. For this reason, and because it was automatically monitored, the first method of water vapour addition was used.

The mass of condensate from the coil after defrosting was also collected, as an additional check on the frost accumulation. This was usually of the order of 60-70% of that added to the system. The difference was attributed to water evaporation during the relatively uncontrolled defrost at the end of each trial. This frost recovery was consistent with values reported by other workers in similar studies (Kondepudi and O'Neal, 1989).

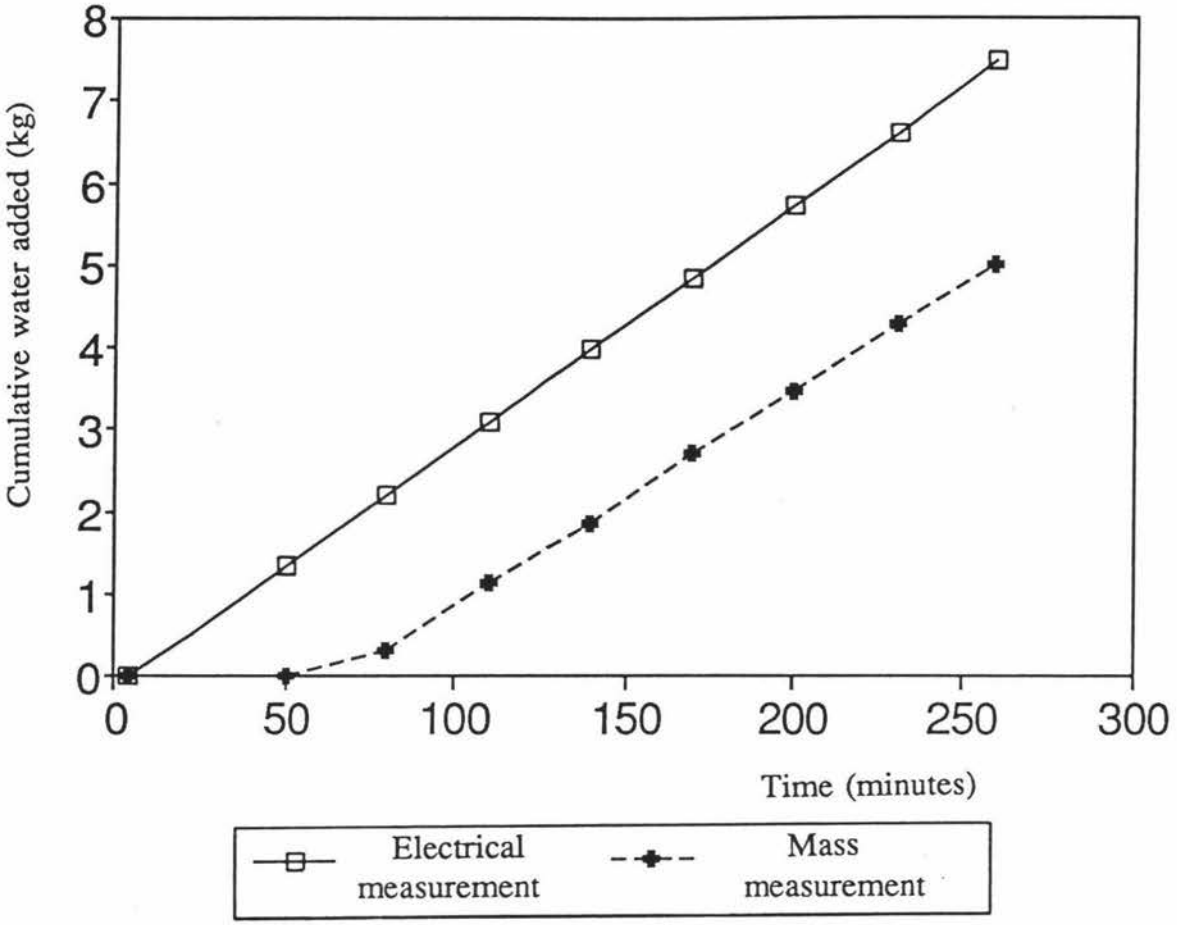

Figure 5.1 Cumulative water addition to the test facility.

5.6 REFRIGERANT THERMODYNAMIC PROPERTIES

The spreadsheet required a number of refrigerant thermodynamic properties to be estimated. The curve fit equations developed for HCFC-22 by Cleland (1986), based on the Chan and Haselden equations of state, were used.

The refrigerant saturated evaporation, or condensation, temperature, $T_{r\,sat}$, was calculated by:

$$T_{r\,sat} = \frac{-2025.4518}{\ln(P_r - 21.25384)} - 248.94 \qquad (5.19)$$

where: P_r = refrigerant pressure (Pa)

$T_{r\,sat}$ = refrigerant saturation evaporation or condensation temperature (°C)

Refrigerant liquid enthalpy, h_r, was given by:

$$h_r = 200 + 1.17036\,T_r + 1.68674\times10^{-3}\,T_r^2 + 5.2703\times10^{-6}\,T_r^3 \qquad (5.20)$$

where: T_r = liquid refrigerant temperature (°C)

Calculation of the refrigerant vapour enthalpy is based on both the refrigerant saturated vapour temperature and the superheat of the vapour.

$$h_r = (250.027 + 0.367265\,T_{sat} - 1.84133\times10^{-3}\,T_{sat}^2 - 1.14556\times10^{-5}\,T_{sat}^3)$$
$$(10^{-3} + 2.85446\times10^{-6}\,T_{SH} + 4.01294\times10^{-10}\,T_{SH}^2 + 1.33612\times10^{-8}\,T_{SH}\,T_{sat} -$$
$$8.11617\times10^{-11}\,T_{sat}\,T_{SH}^2 + 1.411941\times10^{-10}\,T_{sat}^2\,T_{SH} -$$
$$9.53294\times10^{-13}\,T_{sat}^2\,T_{SH}^2) + 155.487 \qquad (5.21)$$

where: T_{SH} = refrigerant vapour superheat (°C)

The refrigerant superheat is the difference between the measured refrigerant vapour temperature, and the saturated evaporation temperature of the refrigerant, taken at the refrigerant pressure, P_r:

$$T_{SH} = T_r - T_{r\,sat} \qquad (5.22)$$

where: T_r = refrigerant vapour temperature (°C)

5.7 AIR PSYCHROMETRIC PROPERTIES

The psychrometric properties of air are required in a number of calculations. The following approximate relationships were used, and are based on the standard assumptions regarding the enthalpy of water vapour discussed by Stoecker and Jones

(1982).

5.7.1 Relative and Absolute Humidity

Absolute humidities were required in a number of energy and mass balances, whilst relative humidity was used for trial comparison purposes.

On the air-on side air dewpoint temperature was measured, whilst relative humidity was measured directly on the air-off side. The air dry bulb temperature was measured on both sides of the coil. The partial, and saturation, pressures of water vapour were then used to calculated the relative and absolute humidities of the air on both sides of the coil as appropriate, as shown below.

The saturated partial pressure of water in air, (vapour pressure of water) was estimated by an Antoine equation, valid for air temperatures below 0°C:

$$p_w = \exp\left[\frac{28.7775 - 6071.67}{T_a + 271.511}\right] \tag{5.23}$$

where: p_w = saturated partial pressure of water in air (Pa)

T_a = air temperature (°C)

The relationships between vapour pressure of water, absolute humidity, and relative humidity, based on the perfect gas laws, are:

$$RH = \frac{100\ p_v}{p_w} \tag{5.24}$$

$$H = \frac{18\ p_v}{29\ (101325 - p_v)} \tag{5.25}$$

where: H = absolute humidity (kg/kg)

p_v = partial pressure of water in air (Pa)

RH = relative humidity (%)

The dew point is the temperature where $p_v = p_w$. Therefore, to find H_{on}, air-on dewpoint, $T_{dp\,on}$, is used in Equation (5.24) to give p_v, which is then used in Equation (5.26). p_w is calculated using T_{on} using Equation (5.26), with air-on relative humidity obtained from Equation (5.25), using p_v and p_w.

For air-off absolute humidity, H_{off}, p_w is estimated using Equation (5.24), which is used in Equation (5.25), with RH_{off}, to find p_v. Finally, p_v is then used in Equation (5.26) to calculate H_{off}.

5.7.5 Air Density

The air density, ρ_a, is based on the air-on temperature and humidity, and was estimated by:

$$\rho_a = \frac{1 + H_{on}}{v_H} \tag{5.26}$$

and

$$v_H = \frac{0.08201\ (273.15 + T_{on})}{(1/29 + H_{on}/18)} \tag{5.27}$$

where: v_H = humid volume (m^3/kg)

5.8 OTHER PARAMETERS

A number of other parameters were estimated, to enable a variety of other coil performance prediction methods to be assessed.

5.8.1 Coil Surface Temperature

The coil surface temperature can be used in a number of calculations, including air enthalpy potential differences calculations. The coil surface temperature was estimated by a ratio of heat transfer coefficients:

$$T_{surf} = \frac{(h_{U\,r}\, A_r\, T_{re}) + (h_{U\,a}\, A_{eff}\, T_{on})SHR^{-1}}{(h_{U\,r}\, A_r) + (h_{U\,a}\, A_{eff})SHR^{-1}} \tag{5.28}$$

where:

A_r = inside area of refrigerant tubes (m^2)

A_{eff} = effective air-side area of the coil (m^2)

$h_{U\,a}$ = air-side heat transfer coefficient (W/m^2 °C)

$h_{U\,r}$ = refrigerant side heat transfer coefficient (W/m^2 °C)

T_{surf} = estimated coil surface temperature (°C)

Correlations used to estimate $h_{U\,r}$ and $h_{U\,a}$ are given in **Appendix** A.2. The effective air-side area was calculated using;

$$A_{eff} = A_a + \eta\, A_f \tag{5.29}$$

where:

Af = fin surface area (m^2)

A_a = outside area of refrigerant tubes (m^2)

η = fin efficiency

Fin efficiency was calculated using a program developed by Hine (1990), to be 0.83 for the coil and the test conditions used in these trials.

5.8.2 Total to Sensible Heat Ratio

By definition the total to sensible heat ratio, *T:S*, is the inverse of the sensible heat ratio. The best estimate of *T:S* was that based on the *SHR* estimate from Equation (5.12):

$$T{:}S = \frac{1}{SHR} \tag{5.30}$$

A number of alternative estimates of the total to sensible heat ratio were also calculated. Firstly, based on air-on and air-off conditions:

$$T{:}S = 1 + \frac{\Delta h_{ig} \, (H_{on} - H_{off})}{c_a \, (T_{on} - T_{off})} \tag{5.31}$$

Although accurate by definition, this was considered to be of dubious experimental accuracy, due to the likely imprecision of, and sensitivity to small changes in, measured humidity values.

Secondly, *T:S* was calculated from measured heat input rates:

$$T{:}S = \frac{\phi_{it}}{\phi_{is}} \tag{5.32}$$

The potential advantage of this method was that any systematic error in measured values would tend to cancel, and have less effect on the *T:S* ratio.

Thirdly, if it is assumed that the air conditions follow a straight line on the psychrometric chart, from the air-on conditions, to the coil surface temperature at the saturation line, then the total to sensible ratio can be estimated from the air-on conditions, and the coil surface temperature and saturation humidity at that temperature (Cleland and Cleland, 1992). The surface temperature used was that estimated using Equation (5.28), and the saturation humidity was calculated using the at the surface temperature:

$$T{:}S = 1 + \frac{h_{ig} \, (H_{on} - H_{sat\ surf})}{c_a \, (T_{on} - T_{surf})} \tag{5.33}$$

where: $H_{sat\ surf}$ = saturation air humidity, calculated at the coil surface temperature (kg/kg)

T_{surf} = coil surface temperature (°C)

Lastly, Cleland and Cleland (1992) suggest the following equation:

$$T{:}S = 1 + \frac{\Delta h_{ig} \, (H_{on} - H_{re\ sat})}{c_a \, (T_{on} - T_{re})} \tag{5.34}$$

where $H_{re\ sat}$ is taken as the saturation humidity calculated at the refrigerant temperature.

This assumes a straight line on the psychrometric chart, as in Equation (5.33), but uses T_{re} as an estimate of the surface temperature, as it is easier to determine in a given system.

6 RESULTS AND DISCUSSION

6.1 PERFORMANCE DECLINE UNDER FROSTING CONDITIONS

Table 4.1 gives the conditions for the 16 trials that were conducted. As defined in Section 5.2, the coil performance parameters of interest were the normalised sensible capacity rating UA/UA_0 , and the normalised air flowrate Q/Q_0. Figures 6.1 and 6.2 show some examples of trends in UA/UA_0 and Q/Q_0 against time. These plots are consistentwith results observed by a number of other investigators with increased relative humidity (low *SHR*) resulting in faster performance decline with time (Ivanova and Gatchilov, 1977; Kondepudi and O'Neal, 1987; and Kondepudi and O'Neal, and 1989). However, with different rates of water addition (and hence frost accumulation) for different trials, it is difficult to compare the performance decline for an equivalent amount of frost accumulation. An alternative comparison of coil performance against total frost accumulation was therefore adopted.

Figures 6.3 and 6.4 shows UA/UA_0 and Q/Q_0 as a function of accumulated frost, M_f, for a number of the trials of various *SHR's*. The drop off in air flowrate and coil performance, for the same amount of frost deposited, was greater at lower *SHR*. This is consistent with the theory proposed by Smith (1989), where it is proposed that the low *SHR* conditions give rise to frost that is less dense and less conductive, which would block the coil quicker, and reduce heat transfer faster for the same frost mass, than under higher *SHR* conditions. There does not appear to be a distinct transition from favourable to unfavourable conditions, but the coarseness of the divisions in *SHR* and trial to trial variability make precise identification of any such transition difficult. Of the trials undertaken, 1-3 appear to be under favourable frosting conditions, 12-16 unfavourable, and 4-11 transitional.

Figures 6.5 to 6.9 show UA/UA_0 and Q/Q_0, as a function of accumulated frost, for all the replicate trials. There was reasonable agreement between replicate trials at higher *SHR* (trials 4-6 and 7-11), but poorer repeatability at lower *SHR* (trials 12-13 and 15-16). Some of the variability is due to heat inputs not being exactly identical,

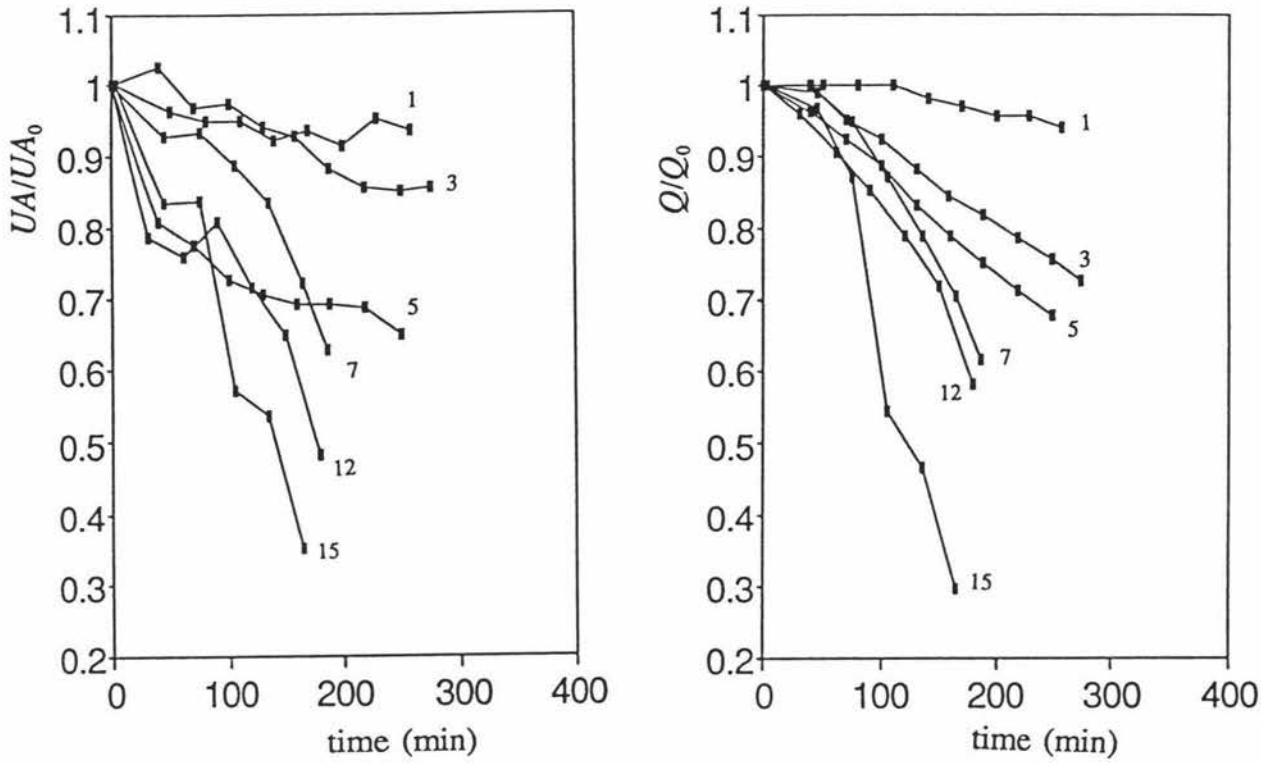

Figure 6.1 Normalised coil sensible capacity ratings and air flowrates as a function of time (Trial numbers indicated).

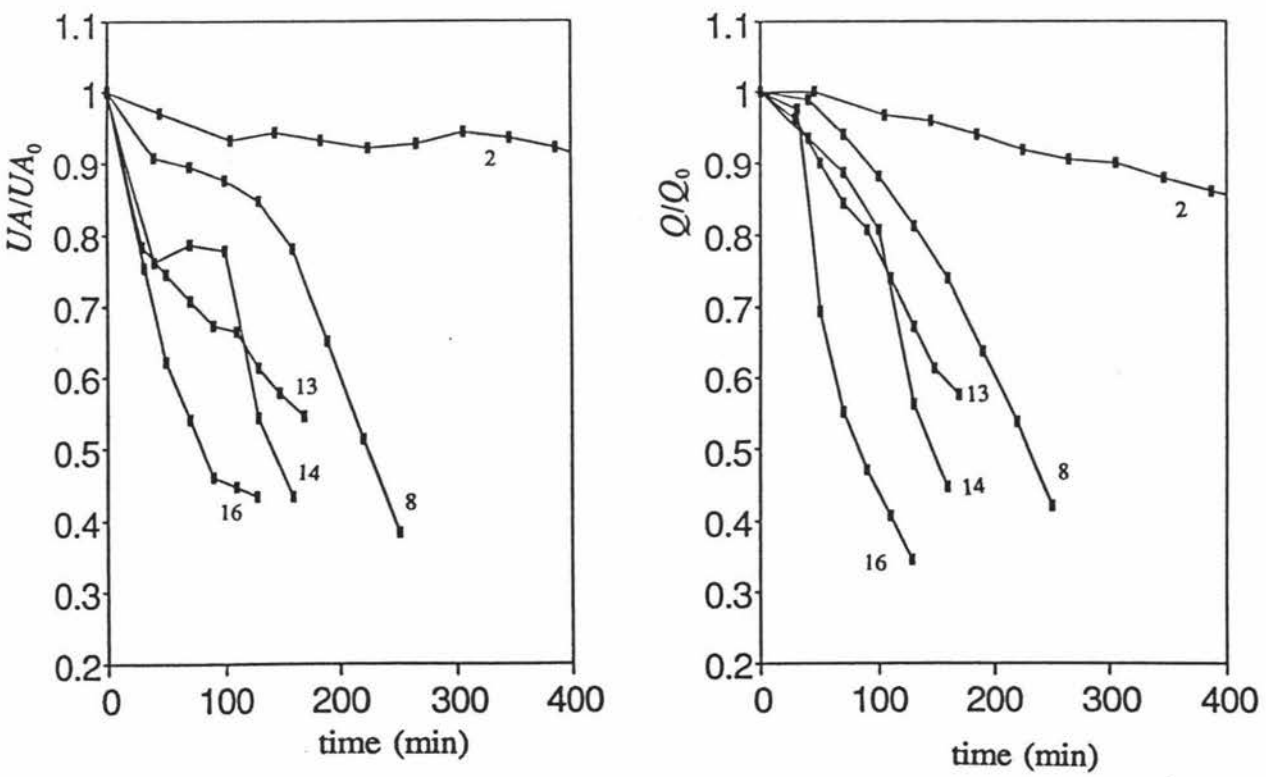

Figure 6.2 Normalised coil sensible capacity ratings and air flowrates as a function of time (Trial numbers indicated).

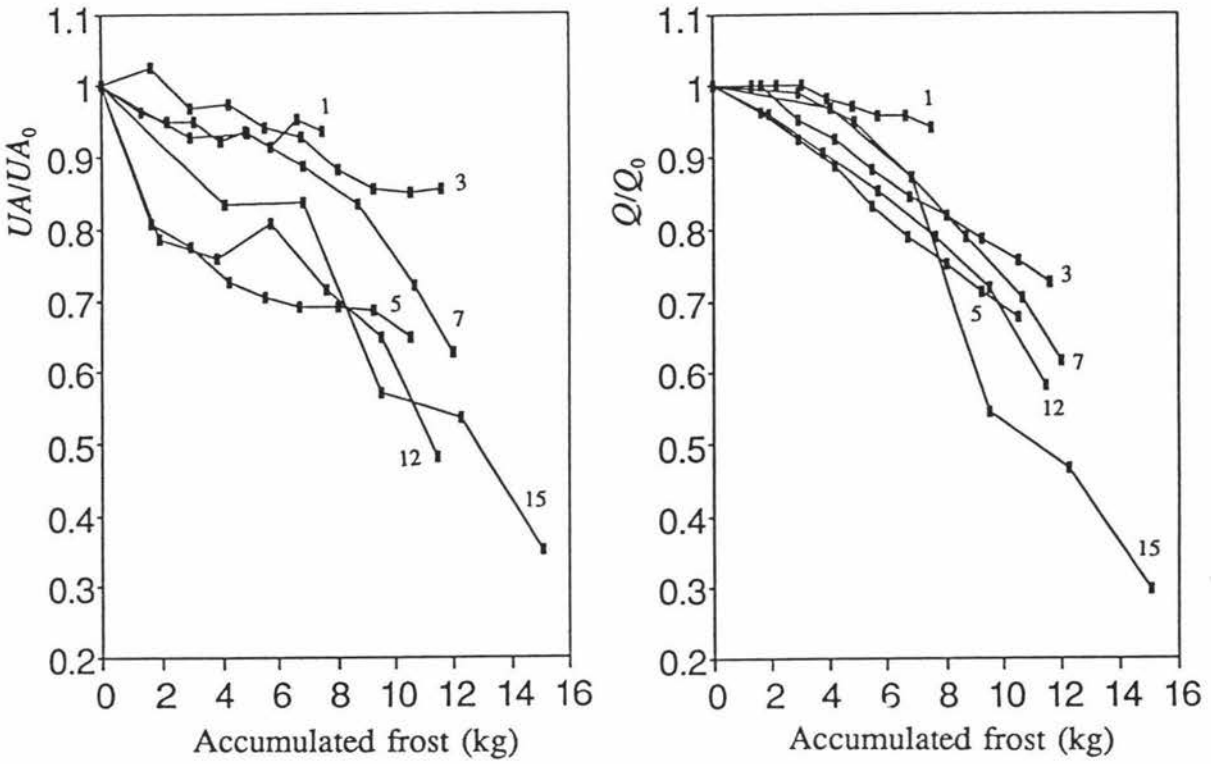

Figure 6.3 Normalised coil sensible capacity ratings and air flowrates as a function of total accumulated frost (Trial numbers indicated).

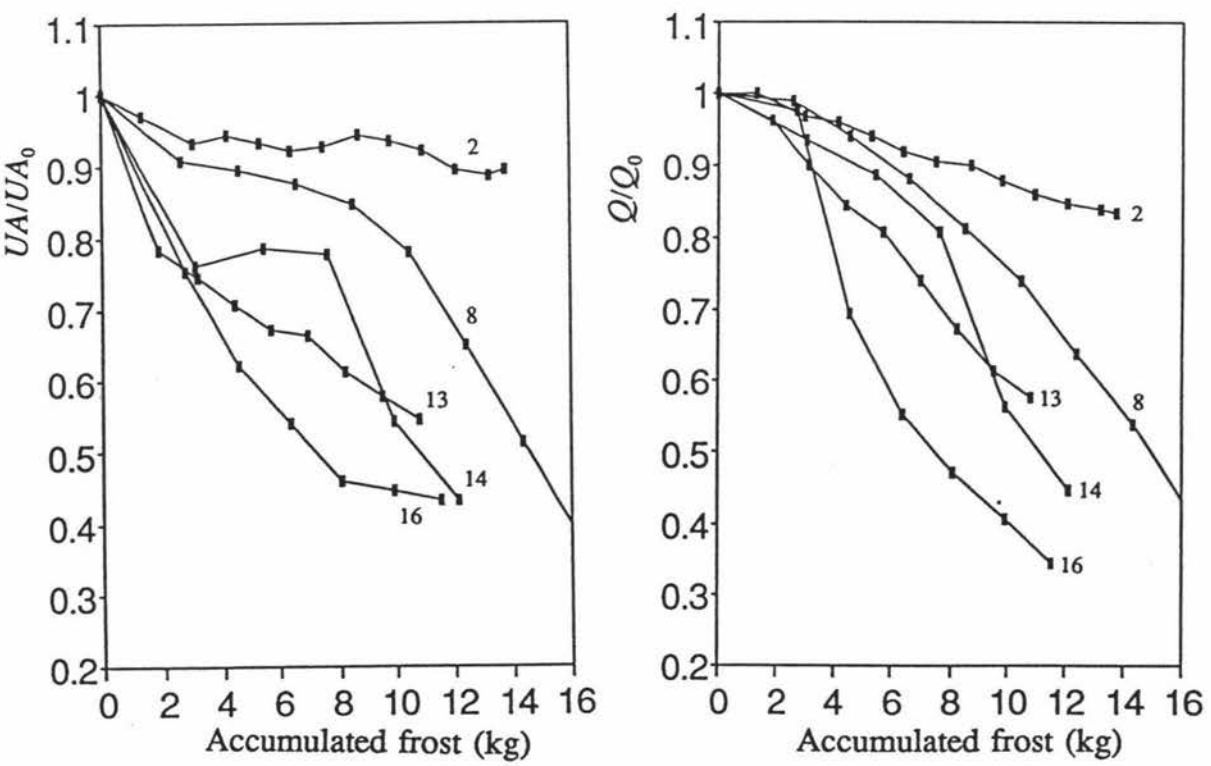

Figure 6.4 Normalised coil sensible capacity ratings and air flowrates as a function of total accumulated frost (Trial numbers indicated).

but it was also observed that frosting was not always uniform across the coil for the low *SHR* trials. Smith (1989) suggested that at the lower *SHR* where unfavourable frost formation was likely to occur, ice crystallisation precipitation in the air was possible. This would result in a far more random frost accumulation process, giving more variable (as well as faster) performance decline.

Figure 6.10 show UA/UA_0 and Q/Q_0 against accumulated frost for all the trials where coil operation was continued with high *SHR* after operation at low *SHR*. The observed recovery in air flowrate and coil performance appeared to be greater for the trials at lower *SHR* (where unfavourable frost formation is more likely) than for the higher *SHR* trial. The recovery may correspond to some remelting and consolidation of low density unfavourable frost into a higher density frost (more favourable).

Figure 6.11 shows Q/Q_0 against UA/UA_0. As the air flowrate declines, so to does the heat transfer, as is reported in the literature (Stoecker, 1957; and Niederer, 1976). There appears to be two groups of data, giving slightly different relationships. One group are trials with higher ϕ_r, whilst the other trials have low ϕ_r. The different relationship between Q/Q_0 and UA/UA_0 can be explained by the increase in the refrigerant-side heat transfer coefficient with increased total heat load. The different ϕ_r for the frosting part of the trial gives different refrigerant-side heat transfer coefficient, which leads to different overall *UA* values, and the two groups result.

Previous work on coil performance with frosting has indicated an initial improvement in heat transfer followed by a decline (Stoecker, 1957; and Kondepudi and O'Neal, 1987). No significant initial enhancement was observed. Either the period of enhancement finished before the first coil performance assessment, or the detrimental effects of frost accumulation quickly exceeded the beneficial effects.

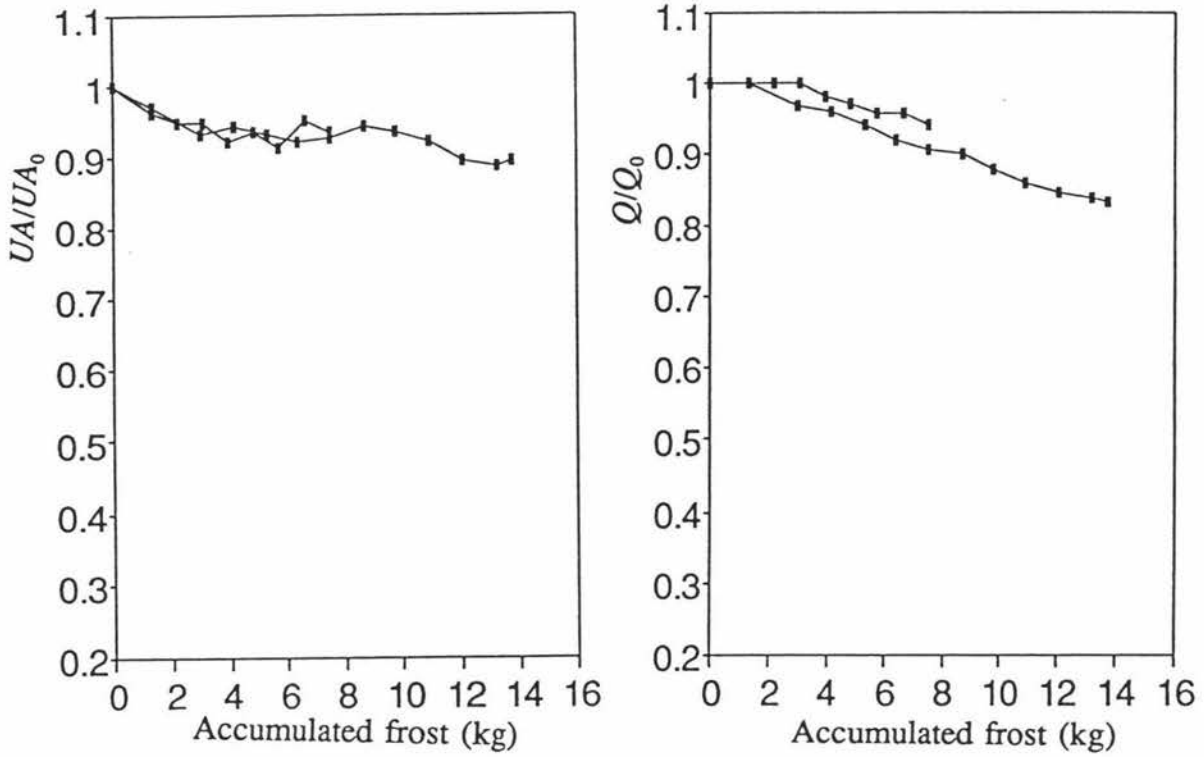

Figure 6.5 Replicates trials of normalised coil sensible capacity rating and air flowrate as a function of total accumulated frost (Trial of *SHR* = 0.84).

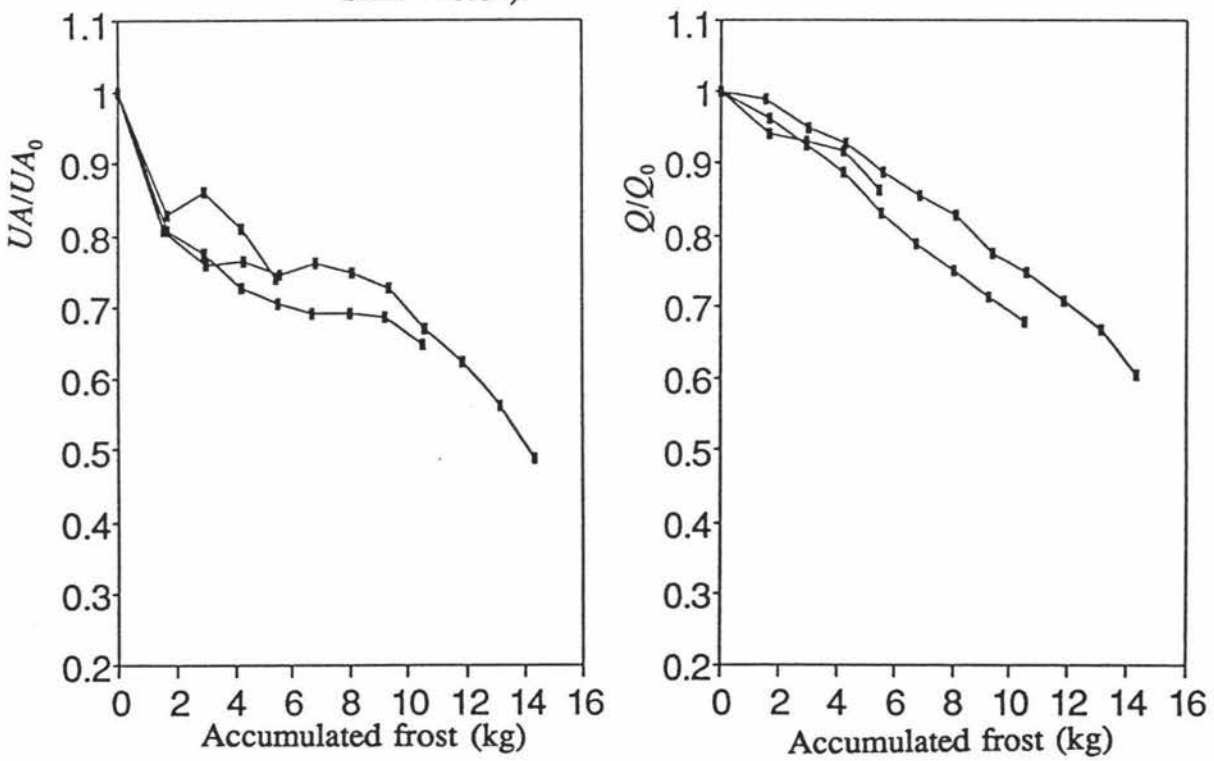

Figure 6.6 Replicates trials of normalised coil sensible capacity rating and air flowrate as a function of total accumulated frost (Trial of *SHR* = 0.71).

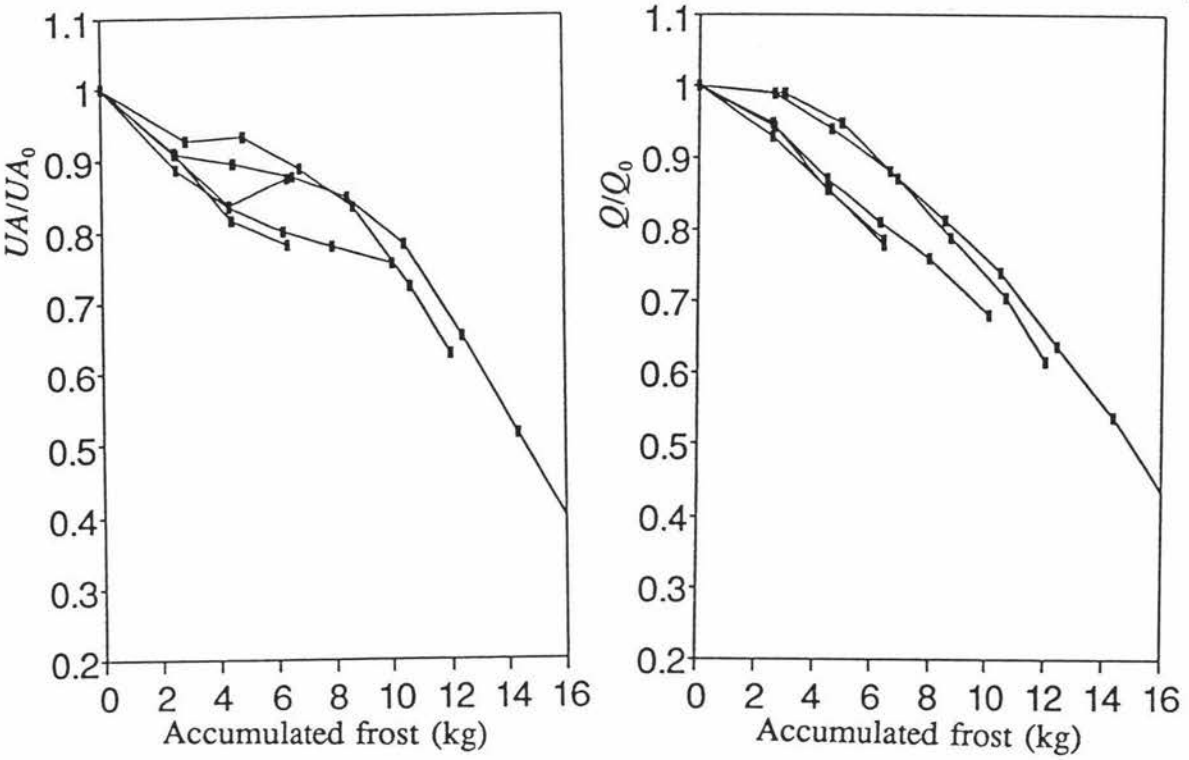

Figure 6.7 Replicates trials of normalised coil sensible capacity rating and air flowrate as a function of total accumulated frost (Trial of *SHR* = 0.70).

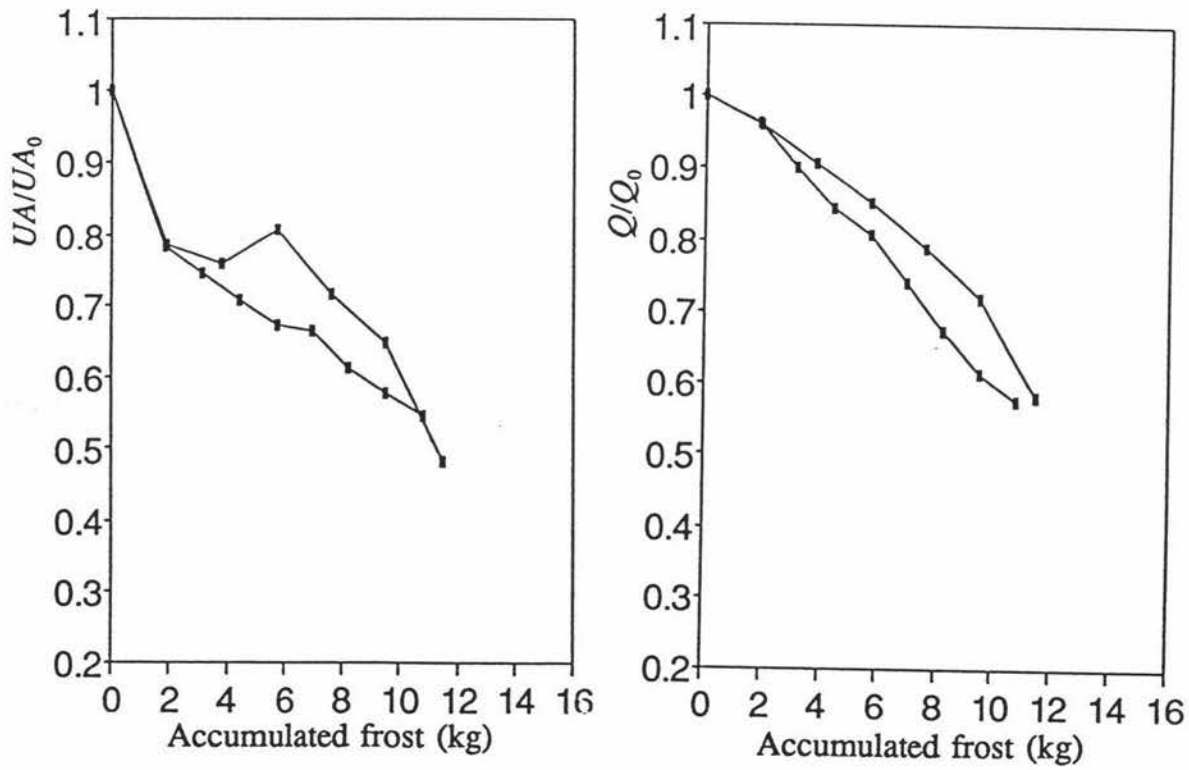

Figure 6.8 Replicates trials of normalised coil sensible capacity rating and air flowrate as a function of total accumulated frost (Trial of *SHR* = 0.62).

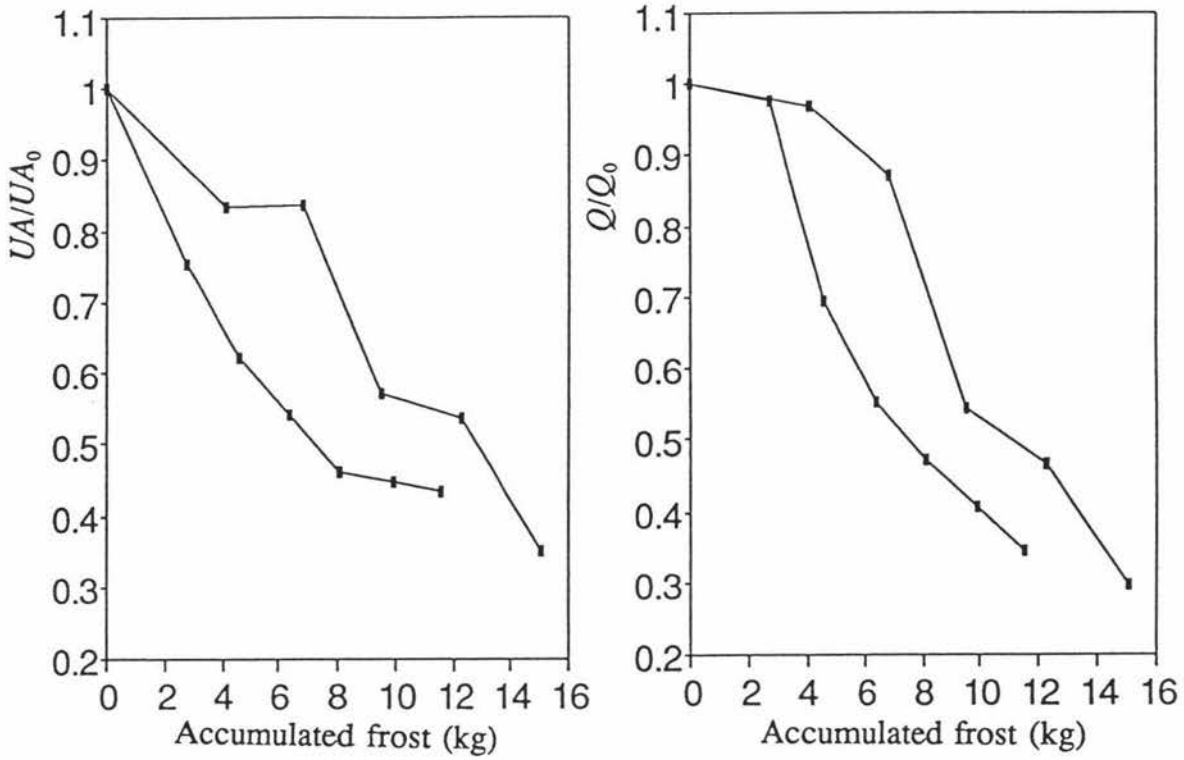

Figure 6.9 Replicates trials of normalised coil sensible capacity rating and air flowrate as a function of total accumulated frost (Trial of $SHR = 0.54$).

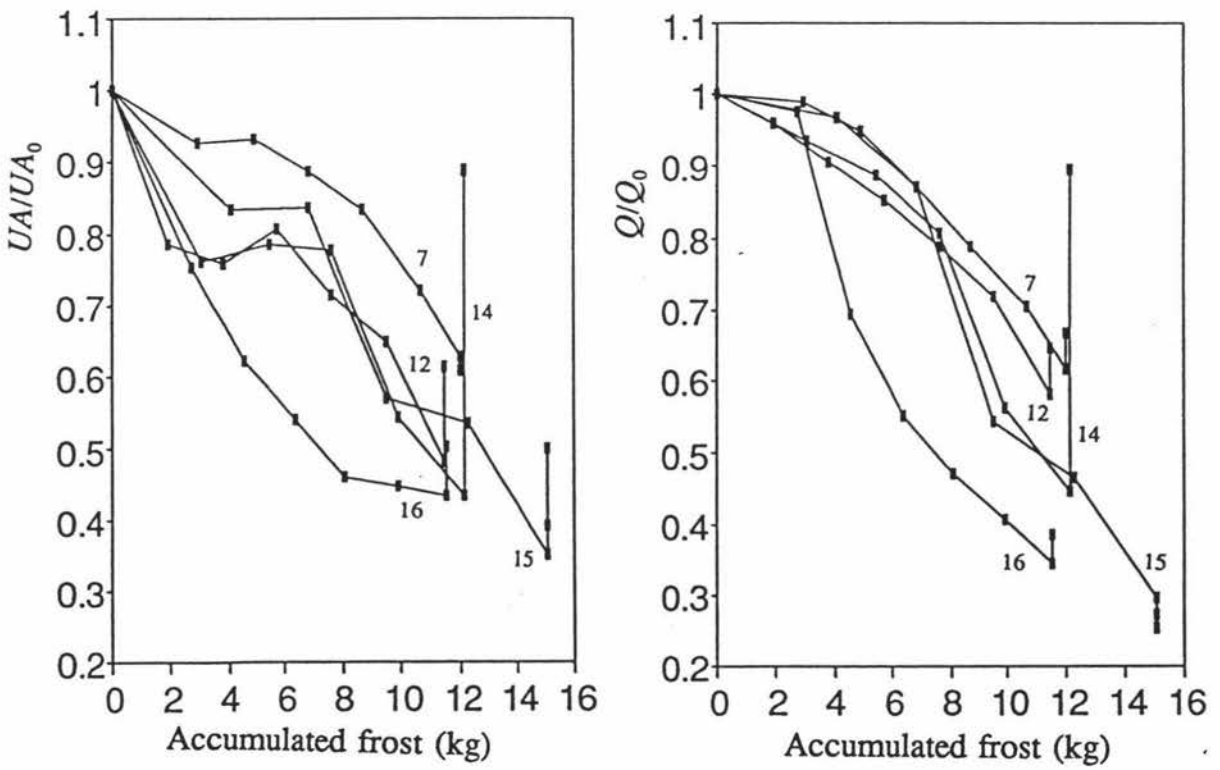

Figure 6.10 Normalised coil sensible capacity rating and air flowrate as a function of total accumulated frost for trials with low *SHR* followed by a high *SHR* recovery period (trial numbers indicated).

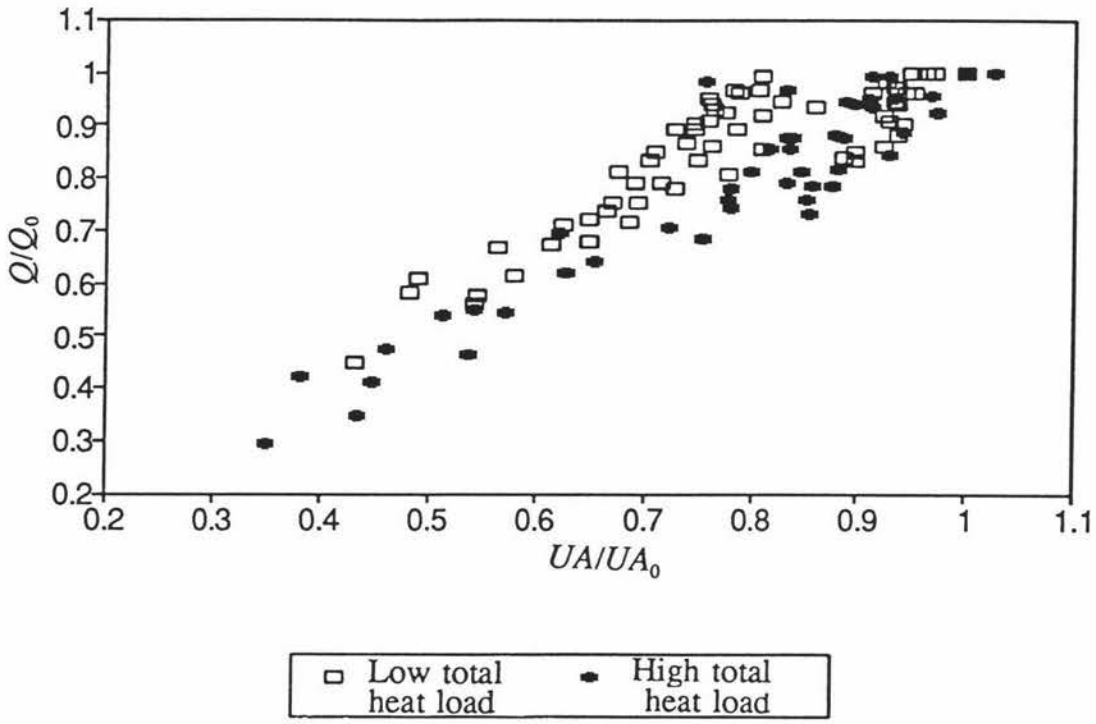

Figure 6.11 Normalised air flowrate as a function of normalised coil sensible capacity rating, for all trials (different total heat loads shown).

6.2 DEFROST PRACTICE

The possibility of both unfavourable frost formation under low *SHR* conditions and recovery of coil performance under high *SHR* conditions, have important implications for the design and operation of coils.

If sustained operation for low *SHR* conditions are expected (such as a fluidized bed pea freezer where product weight loss can typically be 4% at an air temperature of less than -30°C, and the transitional *SHR* is high), then special coil designs may be required to allow continued satisfactory coil performance without high defrost frequency (e.g. low *TD*, large or variable fin spacing).

If low *SHR* conditions only occur for short periods (such as a coil situated near a coldstore door, during door openings) then rapid deterioration in coil performance may occur, but later recovery in performance may allow defrost to be delayed without undue loss of overall system performance.

However, if reasonably long periods of operation at low *SHR* are to followed by long periods at higher *SHR* (such as a beef chiller where evaporative weight loss is high initially but steadily reduces during the chill cycle), then the optimal time for defrost may be in the middle of the cycle when coil operation transitions from unfavourable to favourable frost formation conditions. Defrosting in this manner would not prolong coil operation with low efficiencies.

6.3 RATE OF PERFORMANCE DETERIORATION DUE TO FROSTING

A measure of deterioration was required to test the theory that the rate of performance deterioration will be dependent on *SHR*, as proposed by Smith (1989). That selected was the rate of change of normalised sensible heat transfer coefficient (UA/UA_0) with respect to cumulative frost formation (M_f). The plots of UA/UA_0 versus M_f were not linear as Figures 6.3 to 6.10 show. So the method used to determined the slope of the graph was kept simple. The rate of deterioration was defined as the difference between initial and final performance (excluding any final dry heating only test period), divided by the total mass of frost formed:

$$R_{UA} = -\frac{d\,(UA/UA_0)}{d\,M_f} \approx \frac{UA_0 - UA_{final}}{UA_0\,M_{f\,final}} \qquad (6.1)$$

where:

R_{UA}	=	rate of heat transfer decline with frost acumulation (s/kg)
UA/UA_0	=	normalised coil sensible capacity rating
UA_0	=	initial coil sensible capacity (W/°C)
UA_{final}	=	final measurement of coil sensible capacity rating (W/°C)
M_f	=	mass of frost accumulated on the coil (kg)
$M_{f\,final}$	=	total amount of frost added to coil (kg)

In Figure 6.12 R_{UA} is plotted against *SHR* for all 16 trials. In Figure 6.13 the equivalent plot for air flowrate deterioration is shown, where R_Q is defined as:

$$R_Q = -\frac{d\,(Q/Q_0)}{d\,M_f} \approx \frac{Q_0 - Q_{fin}}{Q_0\,M_{f\,fin}} \qquad (6.2)$$

where:
- R_Q = rate of air flowrate decline with frost accumulation (s/kg)
- Q/Q_0 = normalised air flowrate
- Q_0 = initial air flowrate (m^3/s)
- Q_{final} = final measured air flowrate (m^3/s)

Figure 6.14 shows the relationship between R_{UA} and R_Q. In spite of the crudity of the method used to determine R_{UA} and R_Q the plots show clear trends.

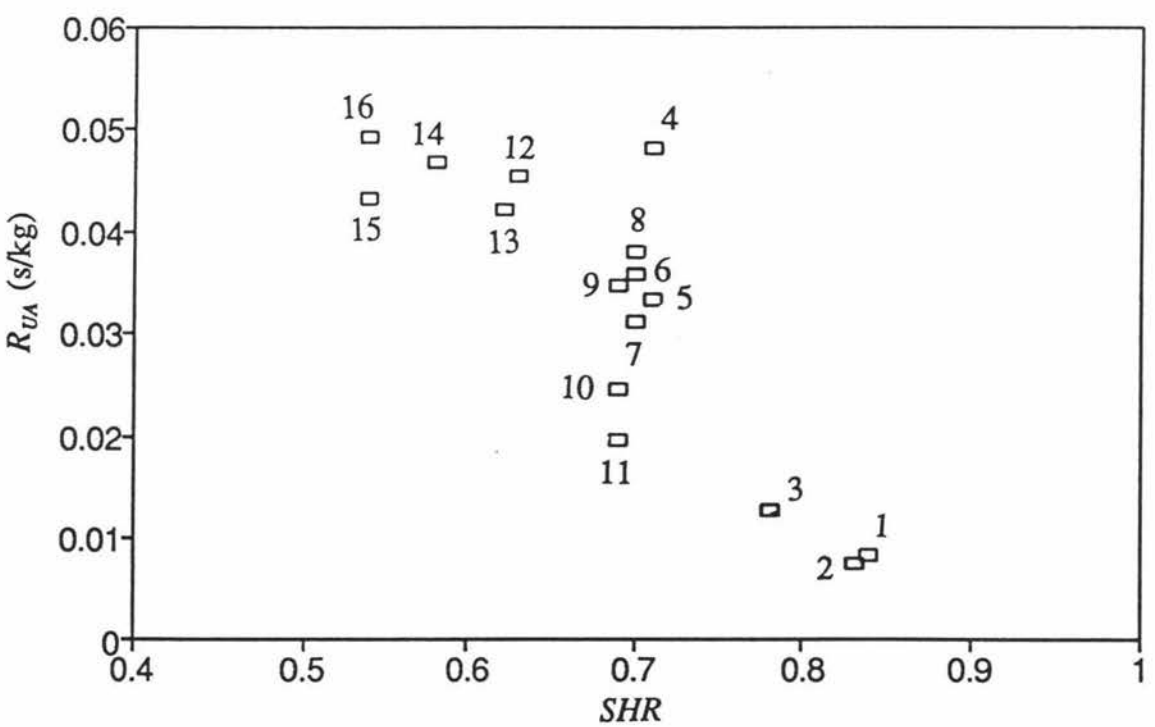

Figure 6.12 Rate of deterioration in coil sensible capacity rating against sensible heat ratio (trial numbers shown).

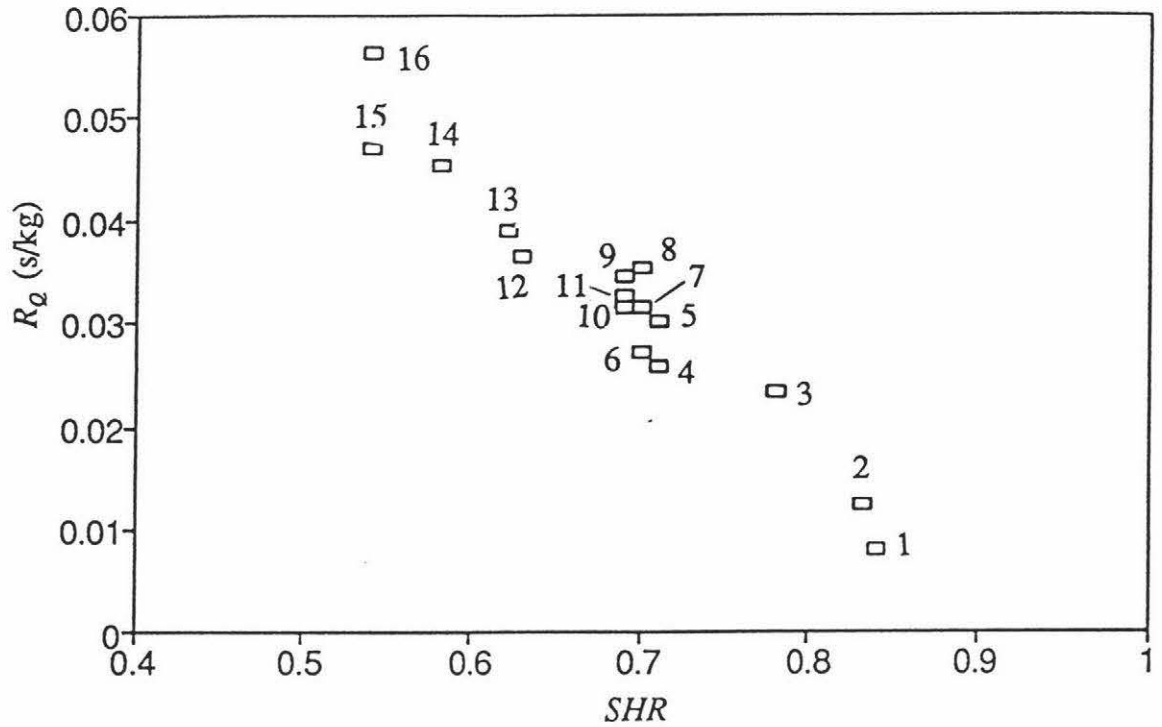

Figure 6.13 Rate of deterioration in air flowrate against sensible heat ratio (trial numbers shown).

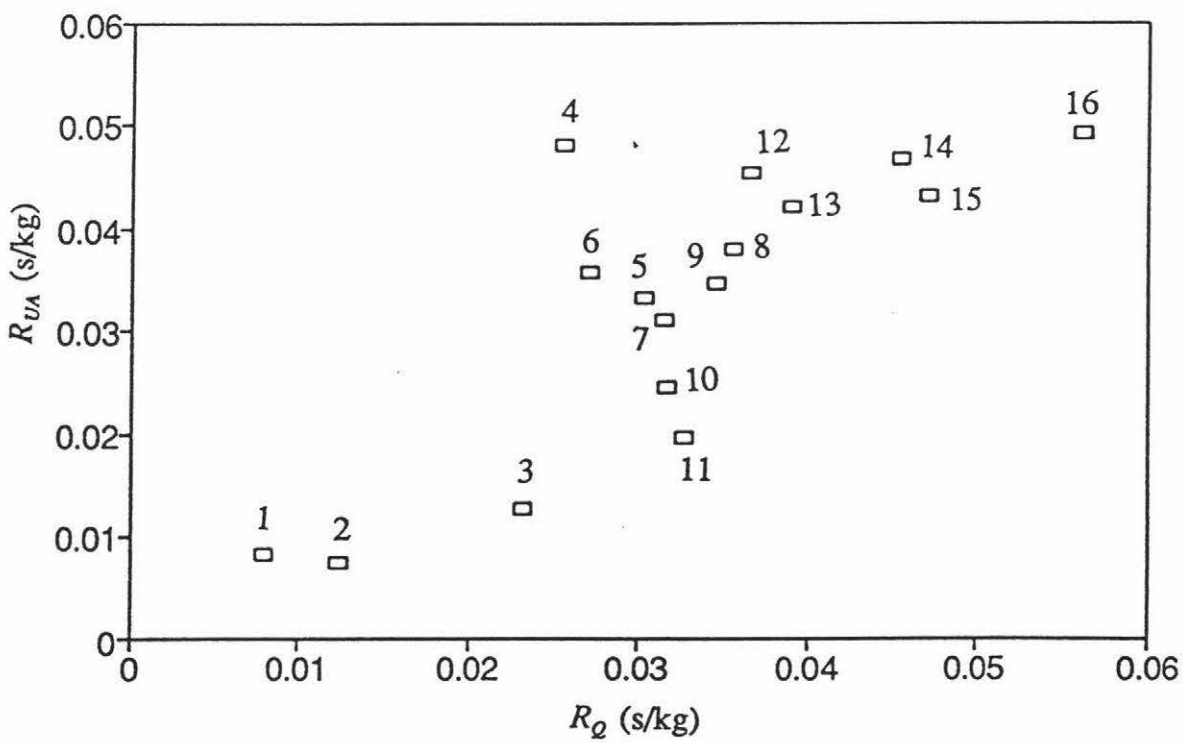

Figure 6.14 Rate of deterioration in coil sensible capacity rating against rate of deterioration in air flowrate (trial numbers shown).

Considering Figure 6.12 first, there are two possible ways in which the plot can be interpreted. The first is that there is an approximately linear relationship with one outlying point, suggesting a gradual transition from low R_{UA} to high R_{UA}, with decreasing *SHR*. The second interpretation is that there is non-linear behaviour as a result of a rapid transition from favourable to unfavourable frost formation. The relationship between R_{UA} and *SHR* (commencing at *SHR* = 1.0 and moving left) is initially a horizontal line on the x axis (whilst coil surface temperature is above the air dewpoint temperature), then a line with low slope in the favourable frost region, followed by a sharply rising line through the transition region (*SHR* $\approx$ 0.7), and finally becoming a relatively flat line for well-developed unfavourable frost conditions (low *SHR*).

Figure 6.13 appears significantly more linear. A high value of R_Q implies that a kilogram of frost at that *SHR* is more restricting on air flow than a kilogram of frost at higher *SHR*. The trend indicates lower frost density at lower *SHR*, but there is no clear evidence of a sharp transition as *SHR* changes. Fig. 6.14 could be explained as either a smooth trend, or as a three part curve with low slope at low R_Q, a steep transition, and then a low slope region at high R_Q.

6.4 PREDICTION OF TRANSITION BETWEEN TYPES OF FROST FORMATION

The fourth aim of the project was to attempt to quantify the transition from favourable to unfavourable frosting conditions. The theory of Smith (1989) suggests that the transition between favourable and unfavourable frost occurs when the line representing air conditions on the psychrometric chart is tangential to the saturation line, at the coil surface temperature. A line above the tangent, which crosses the saturation line, would be expected to give less dense, unfavourable frost formation, where it is proposed that ice crystal precipitation occurs in the air. A line representing the air conditions, passing through the coil, below the tangent would give denser frost, which would be more favourable to coil performance. These conditions are represented on the psychometric chart in Figure 2.1. Given any two

of: air-on temperature (T_{on}), air-on humidity (H_{on}), coil surface temperature (T_s), and *SHR*, it is possible to calculate the remaining conditions and determine the tangent to the saturation line.

At the transitional *SHR* the tangent is given by:

$$\frac{H_{on} - H_{ws}}{T_{on} - T_s} = \frac{dH_{ws}}{dT} \tag{6.3}$$

where: H_{on} = air-on absolute humidity (kg/kg)

H_{ws} = saturation humidity of air at the coil surface temperature (kg/kg)

T_{on} = air-on temperature (°C)

T_s = coil surface temperature (°C)

The absolute humidity can be calculated from the partial pressure of water vapour in the air:

$$H = \frac{18\ p_v}{29\ (p_T - p_v)} \tag{6.4}$$

or

$$p_v = \frac{29\ H\ p_T}{18 + 29H} \tag{6.5}$$

where: H = air absolute humidity (kg/kg)

p_v = partial of water vapour in air (Pa)

p_T = total air pressure (Pa)

The well-known Antoine equation can be used to estimate the relationship between temperature and vapour pressure of water (for $T < 0$°C):

$$p_w \approx \exp\left(28.7775 - \frac{6071.67}{T + 271.511}\right) \tag{6.6}$$

where: p_w = saturation partial pressure or water vapour in air (Pa)

T = air temperature (°C)

and the ratio between actual partial pressure and vapour pressure is the relative humidity:

$$RH = \frac{p_v}{p_w} \approx \frac{H}{H_w} \tag{6.7}$$

where: RH = relative humidity (%)

H_w = saturation humidity (kg/kg)

For saturation at T_s, $p_v = p_w$, $H = H_{ws}$ and Equation (6.5) can be substituted into the left hand version of Equation (6.4) to yield a relationship between H_{ws} and T_s:

$$H_{ws} \approx \frac{1.928300\times10^{7}}{\exp\left(\frac{6071.67}{T_s + 271.511}\right) - 3.106705\times10^{7}} \tag{6.8}$$

Differentiation of this relationship and substitution in Equation (6.3) yields:

$$\frac{H_{on} - H_{ws}}{T_{on} - T_s} \approx \frac{1.1708\times10^{11}\ \exp\left(\frac{6071.67}{T_s + 271.511}\right)}{\left(\exp\left(\frac{6071.67}{T_s + 271.511}\right) - 3.106705\times10^{7}\right)^2 (T_s + 271.511)^2} \tag{6.9}$$

Equations (6.7) and (6.8) are simultaneous equations involving four variables: T_{on}, T_s, H_{on} and H_{ws} which can be solved as required, if any two variables are known. The sensible heat ratio can be defined as:

$$SHR \approx \left(1 + \frac{\Delta h_{ig}\,(H_{on} - H_{off})}{c_a\,(T_{on} - T_{off})}\right)^{-1} \tag{6.10}$$

If it is assumed that the air-on, air-off, and coil surface conditions lie on a straight line on the psychrometric chart (as is normally done for air-conditioning applications in which condensate forms on the coil) then:

$$\frac{H_{on} - H_{off}}{T_{on} - T_{off}} = \frac{H_{on} - H_{ws}}{T_{on} - T_s} \tag{6.11}$$

This result can be substituted in Equation (6.9) to yield:

$$\frac{H_{on} - H_{ws}}{T_{on} - T_s} = \left(\frac{1}{SHR} - 1\right)\frac{c_a}{\Delta h} \tag{6.12}$$

or

$$SHR = \left(1 + \frac{\Delta h_{ig}\,(H_{on} - H_{ws})}{c_a\,(T_{on} - T_s)}\right)^{-1} \tag{6.13}$$

Given an air-on temperature and either the coil surface temperature or the entering air *RH*, it is possible to calculate the critical *SHR*, which forms the tangent to the saturation line on the psychrometric chart. A range of critical *SHR*, have been calculated, as a function of RH_{on}, or T_s, for an air-on temperature of 0°C, and are shown in Table 6.1.

TABLE 6.1 Critical *SHR* for T_{on} = 0°C

RH_{on}	T_{surf}	SHR_{crit}	T_{surf}	RH_{on}	SHR_{crit}
60	-16.4	0.81	-4.0	95.8	0.61
70	-13.2	0.76	-6.0	91.4	0.65
80	-10.1	0.71	-8.0	86.1	0.68
90	-6.7	0.65	-10.0	80.2	0.75
95	-4.7	0.61	-20.0	49.3	0.85

6.5 COMPARISON OF TRANSITION PREDICTION WITH TRIAL RESULTS

The calculation procedure from Section 6.4 was applied to each of the 16 experimental runs. The experimental H_{on} and T_{on} values were substituted into Equations (6.7) and (6.8) to find values of T_s and H_{ws} at the position where the tangent touches the saturation line. These were defined as $T_{s\,tan}$ and $H_{ws\,tan}$. Equation (6.11) could then be used to find the *SHR* for this tangent which is the theoretical transition condition between favourable and unfavourable frost formation. The resulting values are shown in Table 6.2. Also shown in Table 6.2 are measured values of the saturated refrigerant coil exit temperature (T_e), 10 to 20 minutes after the start of frost formation. For practical purposes these can be assumed to be the lowest evaporation temperature in the coil at the start of the frosting trial. Some parts of the coil had evaporation temperatures up to 1°C higher as a result of pressure drop. Typically, T_e dropped by 2 to 3°C through each run.

Refrigerant coil surface temperature is highly variable. On the primary surface (refrigerant tubes) the outer surface temperature will be close to the refrigerant evaporation temperature, but well away from the tubes, the surface will be much

warmer. Therefore if unfavourable frost is to form, it would be expected to initially commence near the tubes. As the tubes become covered with highly insulating frost they will remove less heat, and the fin surface near the tubes will drop in temperature as a result. This fin region may subsequently also form unfavourable frost. Thus if unfavourable frost can initially form on the tubes, the region of unfavourable frosting may enlarge. The critical temperature for the onset of unfavourable frost might therefore be the temperature of the primary surface (refrigerant tubes). This temperature is close to T_e. Figure 6.15 shows the relationship between R_{UA} and (T_e - $T_{s\,tan}$). When T_e is well above $T_{s\,tan}$, the rate of performance deterioration measured by R_{UA} is low, suggestingfavourable frost forms. Conversely, when T_e is well below $T_{s\,tan}$ unfavourable frost forms. When $T_e \approx T_{s\,tan}$ the transition between favourable and unfavourable frost appears to be occurring, but this transition may not be sharp.

Accurate measurement of coil frosting performance is difficult, and the data used here are not of sufficient quality to either prove or disprove the exploratory explanations given. Until better data are available, it is recommended that a comparison of T_e and $T_{s\,tan}$ be used as the best criterion for establishing whether favourable or unfavourable frost will form.

In air conditioning, the mean coil surface temperature is considered the key temperature for defining the extent of dehumidification. The results here suggest that it is the lowest surface temperature rather than the mean surface temperature which defines the type of frost formation.

TABLE 6.2 Predicted transitional frost formation conditions for experimental trials

Trial	T_{on} (°C)	RH_{on} (%)	H_{on} (kg/kg)	SHR	T_e^a (°C)	$T_{s\,tan}$ (°C)	SHR_{tan}
1	-0.2	68	0.00251	0.84	-9.0	-14.0	0.78
2	-0.4	68	0.00247	0.83	-9.7	-14.0	0.78
3	-1.6	72	0.00237	0.78	-11.6	-14.0	0.78
4	-0.8	83	0.00292	0.71	-9.7	-9.9	0.71
5	-1.6	82	0.00270	0.71	-10.1	-11.0	0.73
6	-0.3	82	0.00301	0.71	-8.4	-9.7	0.71
7	0.0	76	0.00286	0.70	-10.5	-11.0	0.74
8	0.2	77	0.00293	0.70	-10.0	-11.0	0.73
9	-0.6	78	0.00279	0.70	-11.4	-11.0	0.74
10	-0.4	81	0.00295	0.70	-10.2	-10.0	0.71
11	-1.4	87	0.00291	0.70	-10.4	-9.0	0.70
12	-0.7	89	0.00316	0.63	-8.9	-7.6	0.67
13	-1.8	87	0.00282	0.62	-11.2	-9.4	0.70
14	-0.1	87	0.00325	0.58	-9.1	-7.8	0.68
15	0.1	93	0.00352	0.54	-10.5	-5.4	0.63
16	0.2	93	0.00355	0.54	-10.6	-5.3	0.63

[a] Value 10 to 20 minutes after frost formation commenced.

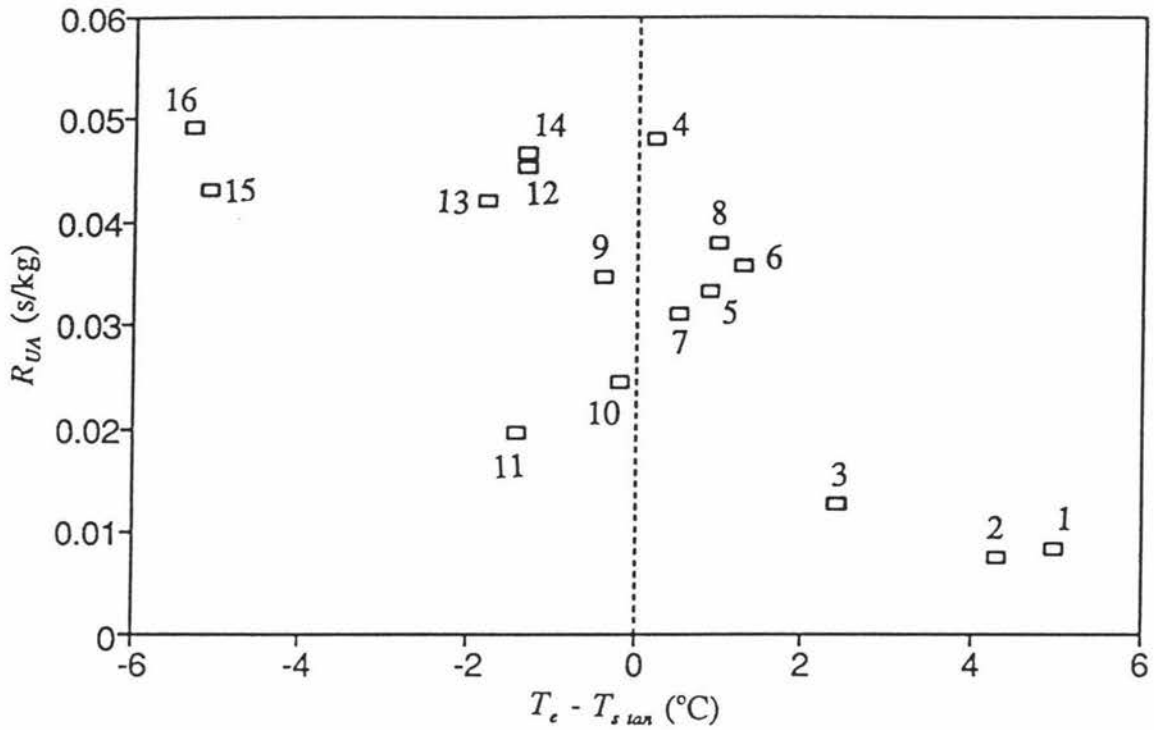

Figure 6.15 Rate of deterioration in coil sensible capacity rating against the difference between the coil evaporation temperature and calculated tangential surface temperature.

7 CONCLUSIONS

The calorimeter style coil test facility allowed coil performance to be measured as frost accumulated in a manner consistent with coil operation in industrial practice. The data collected supported the concept of unfavourable frost formation with a more rapid decline in performance for operation with low *SHR* than that at high *SHR*, for the same total frost accumulation. Some recovery of coil performance was observed when operation at low *SHR* (with rapid deterioration) was followed by a period of high *SHR* operation.

The change in the rate of coil performance deterioration with frost buildup was dependent on *SHR* in a manner consistent with the unfavourable frost formation theory of Smith (1989). The transition between favourable and unfavourable frost formation appears to be related to the lowest temperature on the coil surface rather than the mean temperature. Satisfactory predictions of frost type were obtained by using the refrigerant evaporation temperature as an approximation to the lowest coil surface temperature.

NOMENCLATURE

α	fraction of total load that is sensible
ϕ	heat flow (W)
λ	thermal conductivity (W/m°C)
η	fin efficiency
A	area (m^2)
c	specific heat capacity (J/kg°C)
E	insulation effectiveness
h	enthalpy (J/kg)
h	heat transfer coefficient ($W/m^{2o}C$)
Δh	latent heat (J/kg)
H	air absolute humidity (kg/kg)
k	heat loss factor ($W/m^{2o}C$)
$LMED$	log mean enthalpy difference
m	mass flowrate (kg/s)
p	partial pressure (Pa)
P	pressure (Pa)
PF	power factor
Q	air flowrate (m^3/s)
R	rate of performance deterioration per kg of accumulated frost
RH	air relative humidity (%)
SHR	sensible heat ratio
T	temperature (°C)
TD	temperature difference between air and refrigerant(°C)
$T:S$	total to sensible heat ratio
U	overall heat transfer coefficient (W/m^2 °C)
UA	coil sensible capacity rating (W/°C)
v	air velocity (m/s)
v_H	air humid volume (m^3/kg)
x	tube thickness (m)

Subscripts

0	initial, first
a	air
am	ambient
c	condenser
crit	critical
d	dry heater
dp	dew point
e	evaporator, evaporation
eff	effective
f	fan
fg	liquid to gas transition
fin	fin
final	at the completion of the frosting period
h	humidifier
i	inlet
ig	solid to gas transition
l	latent
loss	heat losses
m	mean
meas	measured
off	air-off side
on	air-on side
o	outlet
p	pipe
Q	air flowrate
r	refrigerant
s	sensible
sat	saturated
SH	superheat
surf	surface

t	total
U	heat transfer coefficient
UA	coil sensible capacity rating
v	valve
v	vapour
w	water

REFERENCES

Beatty K.O., Finch E.B., Schoenborn E.M. (1951): Heat transfer from humid air to metal under frosting conditions. *Refrigeration Engineering.* **59** 1203-1207.

Brian P.L.T., Reid R.C., Shah Y.T. (1970): Frost deposition on cold surfaces. *Ind. Eng. Chem. Fund.* **9** (3) 375-380.

Chung P.M., Aldren A.B. (1953): Frost formation and heat transfer on a cylinder surface in humid air flow; part I. *Heating, Piping, and Air Conditioning.* **30** (9).

Chung P.M., Aldren A.B. (1953): Frost formation and heat transfer on a cylinder surface in humid air flow; part II. *Heating, Piping, and Air Conditioning.* **30** (10).

Cleland A.C. (1986): Computer subroutines for rapid evaluation of refrigerant thermodynamic properties. *Int. J. Refrig.* **9** 346-351.

Cleland A.C., Cleland D.J. (1992): *Cost-Effective Refrigeration.* Massey University, Palmerston North, New Zealand.

Cooper J.R., Le Fevre E.J. (1986): *Thermophysical Properties of Water Substance.* Edward Arnold.

Domanski P., Didion D. (1984): Mathematical model of an air-to-air heat pump equiped with a capillary tube. *Int. J. Refrig.* **7** 249-255.

Gatchilov T.S., Ivanova V.S. (1977): Characteristics of extended surface air coolers during exploitation under frosting conditions. *Refrig. Sci. and Technology.* **1977-4** 101-106.

Gatchilov T.S., Ivanova V.S. (1979a): Characteristics of the frost formed on the surface of the finned air coolers. *Proc. XV Int. Congr. Refrig.* **2** 997-1003.

Gatchilov T.S., Ivanova V.S. (1979b): Characteristics of extended surface air coolers during operation under frosting conditions. *Int. J. Refrig.* **2** 233-236.

Gates R.R., Sepsy C.F., Huffman G.D. (1967): Heat transfer and pressure loss in extended surface heat exchangers operating under frosting conditions. *ASHRAE Trans.* **73** (2) I.2.1-I.2.13.

Goldstein P.E. (1983): A mathematically complete analysis of plate-fin heat exchangers. *ASHRAE Trans.* **89** (2A) 447-470.

Gray D.L., Webb R.L. (1986): Heat transfer and friction correlation for finned tube heat exchangers having plain fins. *8th ASME Int. Heat Trans. Conf.* San Francisco.

Greenspan L. (1977): Humidity fixed points of binary saturated aqueous solutions. *Journal of Research of the National Bureau of Standards.* **81A** (1) 89-96.

Haukas H.T. (1983): Calculation of gravity fed evaporators. *Proc. XVI Int. Congr. Refrig.* **1983-2** 1067-1073

Hayashi Y., Aoki K., Yuhara H. (1977): Study of frost formation based on a theoretical model of the frost layer. *Heat Transfer Jap. Res.* **6** (3) 79-94.

Hayashi Y., Aoki A., Adachi S., Hori K. (1977): Study of frost properties correlating with frost formation types. *J. Heat Transfer.* **99** (2) 239-245.

Hosoda T., Uzuhashi H. (1967): Effects of frost on heat transfer coefficient. *Hitachi Review.* **16** (6) 254-259.

Infante Ferreira C.A. (1988): Dutch standard for testing air coolers. *Refrig. Sci. and Technology.* **1988-5** 7.1-7.6.

Ivanova V.S., Gatchilov T.S. (1975): Some aspects of frost formation on extended surface air coolers. *Proc. XIV Int. Congr. Refrig.* **2** 625-632.

Ivanova V.S., Gatchilov T.S. (1983): Analysis of air coolers performance at frost formation conditions. *Proc. XVI Int. Congr. Refrig.* **3** 877-883.

Jones B.W., Parker J.D. (1975): Frost formation with varying environmental parameters. *J. Heat Transfer.* **97** (2) 255-259.

Jung D., Radermacher R. (1993): Prediction of evaporation heat transfer coefficient and pressure drop of refrigerant mixtures in horizontal tubes. *Int. J. Refrig.* **16** 201-209.

Kamai S., Mizushina S., Kifune S., Koto T. (1952): Research on frost formation in a low temperature cooler condenser. *The Japan Science Review.* **2** (3).

Kays W., London A.L. (1964): *Compact Heat Exchangers.* McGraw Hill Publishing.

Kondepudi S.N., O'Neal D.L. (1987): The effects of frost growth on extended surface heat exchanger performance: A review. *ASHRAE Trans.* **93** (2) 258-274.

Kondepudi S.N., O'Neal D.L. (1989): Effect of frost growth on the performance of louvered finned tube heat exchangers. *Int. J. Refrig.* **12** 151-158.

Kondepudi S.N., O'Neal D.L. (1993a): Performance of finned-tube heat exchangers under frosting conditions: I. Simulation model. *Int. J. Refrig.* **16** 175-180.

Kondepudi S.N., O'Neal D.L. (1993b): Performance of finned-tube heat exchangers under frosting conditions: II. Comparison of experimental data with model. *Int. J. Refrig.* **16** 181-184.

Lotz H. (1971): Heat and mass transfer and pressure drop in frosting finned coils. *Proc. XII Int. Congr. Refrig.* **2** 499-505.

Marinyuk B.T. (1980): Heat and mass transfer under frosting conditions. *Int. J. Refrig.* **3** 366-368.

Nesje O.M., Skaugen G. (1989): General computer program for simulation of air coolers. *Refrig. Sci. and Technology.* **1989-1** 315-322.

Netherlands Standard Institute (1979): *Determination of the performance of frosted air coolers with forced air circulation.* NEN 1876. 1st edition.

Niederer D.H. (1976): Frosting and defrosting effects on coil heat transfer. *ASHRAE Trans.* **82** (1) 467-473.

Ogawa K., Tanaka N., Takeshita M. (1993): Performance improvement of plate fin-and-tube heat exchangers under frosting conditions. *ASHRAE Trans.* Preprint **CH-93-2-4.**

O'Neal D.L., Tree D.R. (1985): A review of frost formation in simple geometries. *ASHRAE Trans.* **91** (2a) 267-281.

Parish H.C., Sepsy C.F. (1972): A numerical analysis of frost formation under forced convection. *ASHRAE Trans.* **78** (1) 236-251.

Poredos A., Gaspersic (1987): Investigation of direct expansion fin coils by calculation and measurements. *Proc. XVII Int. Congr. Refrig.* **2** 316-322

Sanders C. Th. (1972): Testing of air coolers operating under frosting conditions. *Refrig. Sci. and Technology.* **1972-1** 383-398.

Sanders C. Th. (1974): *Frost formation: The influence of frost formation and defrosting on performance of air coolers*. Ph.D. Dissertation, Delft University, Oct 1974.

Schneider H.W. (1972): Transfered mass and density of frost formed on a cylindrical tube in cross flow. *Refrig. Sci. and Technology*. **1972-1** 149-155.

Schneider H.W. (1978): Equations of the growth rate of frost forming on cooled surfaces. *Int. J. Heat Mass Transfer*. **21** 1019-1024

Shah M.M. (1976): A new correlation for heat transfer during boiling flow through pipes. *ASHRAE Trans*. **82** (1) 66-86.

Smith G.R. (1989): Theoretical cooling coil calculations at freezer temperatures to avoid unfavourable coil-frost. *ASHRAE Trans*. **95** (2) 1138-1148.

Steiner D. (1983): Flow boiling heat transfer for refrigerants and cryogenic fluids inside tubes. *Proc. XVI Int. Congr. Refrig*. **1983-2** 139-145.

Stoecker W.F. (1957): How frost formation on refrigeration coils affects refrigeration systems. *Refrigerating Engineering*. **65** (2) 42-46.

Stoecker W.F. (1960): Frost formation on refrigeration coils. *ASHRAE Trans*. **66** 91-103.

Stoecker W.F. (1967): How frost formation on refrigeration coils affects operation in refrigerated warehouses. *Quick Frozen Foods*. (6) 125-127.

Stoecker W.F., Jones J.W. (1982): *Refrigeration and Air Conditioning*. Second edition, McGraw-Hill Book Company, New York.

Taplin L.E. (1964): Effect of frost on extended surface evaporators. *AIRAH Trans.* **18** (8) 28-35.

Turaga M., Guy R.W. (1985): Refrigerant side heat transfer and pressure drop estimates for direct expansion coils. A review of works in North American use. *Int. J. Refrig.* **8** 134-141.

Turaga M., Lin S., Fazio P.P. (1988): Correlations for heat transfer and pressure drop factors for direct expansion air cooling and dehumidifying coils. *ASHRAE Trans.* **94** (2) 616-630.

Webb R.L. (1980): Air-side heat transfer in finned tube heat exchangers. *Heat transfer Eng.* **1** (3) 33-49.

Wile D.D. (1966): Role of the evaporator in maintaining high humidity. *ASHRAE J.* **8** (12) 67-70.

Yamagishi K., Karaki A. (1975): New method of static analysis for a chilled water cooling and dehumidifying coil. *Heat Transfer Jap. Res.* **4** (3) 70-96.

APPENDIX A

A.1 Air and Refrigerant Side Heat Transfer Coefficients

Correlations for both the air and refrigerant side heat transfer coefficients had previously been estimated, under dry conditions, for the test coil used (Hine 1990; O'Hagan, 1992). For simplicity it was assumed that the air-side heat transfer coefficient would not be affected by frost accumulation on the coil surface.

The correlation for the air-side heat transfer coefficient, appropriate for the test coil that was used, is:

$$h_{U\,a} = 41.3(v_a)^{0.7} \tag{A.1}$$

where: $h_{U\,a}$ = air-side heat transfer coefficient (W/m^2 °C)

v_a = coil air face velocity (m/s)

Given the overall heat transfer coefficient had been calculated using Equation (5.1), it is possible to back calculate the refrigerant-side heat transfer coefficient, using the above correlation for air-side heat transfer coefficient, and equation 2.9. Data calculated in this way was used and the following correlation for the refrigerant-side heat transfer coefficient was developed:

$$h_{U\,r} = 5.606\left[\frac{\phi_t}{A_r}\right]^{0.518} \tag{A.2}$$

where: $h_{U\,r}$ = refrigerant side heat transfer coefficient (W/m^2 °C)

A_r = inside area of refrigerant tubes (m^2)

ϕ_t = total heat load (W)

A.2 Analysis Output for Trial 2 After 346 Minutes

. RAW DATA ANALYSIS.

	TEMP1-O	TEMP2-O	TEMP3-O	TEMP4-O	TEMP5-O	TEMP6-O	TEMP7-O	TEMP8-O	TEMP10-O	TEMP11-O	TEMP12-O	TEMP13-O	TEMP14-O
rg	18.42233	-10.928	-1.75133	-11.2147	-5.66367	-9.85467	-3.632	-10.331	-11.4087	-11.1193	26.763	14.19967	17.968
ax	18.69	-10.81	-1.58	-11.06	-5.4	-9.7	-3.42	-10.16	-11.19	-10.93	26.93	14.54	18.08
in	18.2	-11.06	-1.9	-11.39	-5.78	-10.03	-3.74	-10.48	-11.58	-11.33	26.57	13.99	17.78
d	0.122163	0.097447	0.092113	0.080072	0.088185	0.062436	0.091775	0.071803	0.09036	0.098113	0.067683	0.124806	0.096416
	ambient	ref in	ref out	ref in	ref out	ref in	ref out	ref mid	ref mid	ref mid	cond Rin bitzer	con Rout bitzer	cond Win bitzer

	TEMP15-O	TEMP16-O	TEMP17-O	TEMP18-O	TEMP19-O	TEMP20-O	TEMP21-O	TEMP22-O	TEMP23-O	TEMP24-O	TEMP26-O	TEMP27-O	TEMP28-O
g	26.191	23.204	-1.03633	-0.46867	-0.546	-2.87467	-3.22533	-3.17633	-0.28467	-0.575	-0.257	-0.64433	-0.52867
ix	26.4	23.28	-0.82	-0.38	-0.44	-2.72	-3.04	-2.91	-0.13	-0.38	-0.13	-0.5	-0.44
n	26.04	23.1	-1.26	-0.64	-0.75	-3.04	-3.35	-3.35	-0.45	-0.7	-0.38	-0.75	-0.64
	0.079429	0.067409	0.104833	0.068641	0.095589	0.077749	0.068153	0.099515	0.086554	0.083775	0.04981	0.077403	0.057835
	con Wout new	R pre EX	air on	tunnel	tunnel	air off	air off	air off	air on	air on	air on	air on	air on

	TEMP29-O	TEMP30-O	TEMP31-O	TEMP32-O	PT1-C	PT2-C	PT3-C	PT4-C	PT6-I	PT7-I	PT8-I	PT9-I	PT10-I
l	-3.24767	-3.20733	-3.446	0	0.188	-0.52067	1.305667	-2.85667	-3.05	-3.04333	27.31	16.07	-2.96333
c	-3.1	-3.04	-3.23	0	0.25	-0.47	1.52	-2.77	-2.96	-2.96	27.4	16.07	-2.96
	-3.35	-3.35	-3.61	0	0.06	-0.66	1.13	-2.97	-3.06	-3.06	27.3	16.07	-3.06
	0.079945	0.080454	0.101541	0	0.074404	0.084021	0.112526	0.099107	0.03	0.037268	0.03	7.89E-09	0.017951
	air off	air off	air off	air off	air on	air on	tunnel	air off	air off	air off	Ref outCon new	Win cond new	air off

	PT11-I	PT12-I	PR1-I	PR2-I	PR3-I	PR4-I	PR5-I	PR6-I	POWER	POWER2	RHS-I	VOLTAGE	PT5-C
	70.88967	0.54	10.2	10.11	3.424333	2.26	0.92	2.394	5565	1417.5	0.04495	234.1	96.41
	74.06	0.54	10.2	10.11	3.47	2.26	0.92	2.4	5615	1426	0.0451	235	96.45
	67.29	0.54	10.2	10.11	3.39	2.26	0.92	2.38	5545	1414	0.0448	234	96.25
	2.282689	0	5.44E-09	ERR	0.022013	ERR	3.4E-10	0.00611	21.43984	3.694591	0.000112	0.3	0.08
a	new com	new com	1121.325 aft Cond	1112.325 pre EX	443.7583 aft EX	327.325 aft EVP	193.325 aft KVQ	340.725 aft Dist	element		Ref flow		ref inCon new

	RH1-C	RH2-C	RH3-C	RH4-C	Fan I
	-4.645	78.2	-2.5	80.77	1.375743
	-4.63	78.33	-2.5	80.77	1.3826
	-4.78	78.18	-2.5	80.77	1.3733
	0.045	0.05099	0	3.77E-08	0.00301
	Dew pt on	rh-OFF	SPARE	rh-off	Fan current

NUMBER OF SAMPLE 51

MPERATURE, HUMIDITY AND PRESSURE CALCULATIONS.

Ton Temp of air entering evaporator
= -0.47 (no c141)

Toff(m)= -3.11 measured air off temp

Toff -3.28 actual air off temp

Ef = 0.5 fan efficiency

Ambient air temp = 18.42

Grids temps

-0.28	0.19	-0.26
	-0.58	-0.47
-0.64	-0.53	
-3.25		-3.45
-3.04	-2.96	-3.05
-3.21		

(no j148,h141)

Others in room

-1.04	-0.52
-0.55	
-2.87	-3.18
-3.23	-2.86

HUMIDITIES

Calculations samples

RH-on:	68.06	Ton =	-0.47	Dewpt on=	-5.045
H-on:	0.00246				
RH-off:	79.49	78.20	80.77		
H-off:	0.002304				

Partial pressures

pd(pv)	400.0506	for less tha
pw	587.8214	
pv	374.7802	
pw	471.5106	

Refrigerant evap. temps per 3 circuits

circuit	Tri	Trm	Tro	superheat
1	-10.93	-11.12	-1.75	
2	-11.21	-11.41	-5.66	
3	-9.85	-10.33	-3.63	
ave	-10.67	-10.95	-2.69	9.50
SST	-11.07		-12.19	

REFRIGERANT PRESSURES

	Pressure	Ave	PressDrop	Range	pres(KPa)	SST
comp dischg(psi g)	157.000					
comp dischg(bar a)	11.838				1183.8	29.68
after cond (Prco)	11.213				1121.3	27.62
Pre Expansion(Prvi)	11.123				1112.3	27.31
Pre Distributer(Prvo)	4.436				443.8	-3.45
Pre Evap(Pri)	3.407	3.340	0.134		340.7	-11.07
Post Evap(Pro)	3.273				327.3	-12.19
After KVQ	1.933			0.000	193.3	-25.91

ENSOR HEAT BALANCE.

Cooling water heat balance

Twi:	16.07	C
Two:	26.477	C
Tdiff:	10.407	C
H2O flow	0.234	kg/s (Mw)

Cooling water flow:

run	wt(g)	time(s)	rate(kg/s)
1	5878	25	0.2350
2	5796	25	0.2319
3	5866	25	0.2346

CONDENSER AMBIENT LOSSES

W ends

area	0.033393
Tdiff	43.43767
heatloss	1.899934
	new comp

Cp:	4181.9			4			
Qw	10178.12	watts		5			
CondLoss	0.00	watts	ave	5846.667	25	0.2339	(Mw)
Qw+CD=	10178.12	watts					

Refrigerant heat balance

Trci:	96.41	C	Trco:	27.31	C
Pdis:	11.84	bar a	Prco:	11.21	bar a
SST@Pr.V:	29.68		SST@Pr.L:	27.62	
Superheat	66.73	C	Subcool:	0.31	C
hrci:	469.55	J/Kg	hrco:	233.33	J/Kg

hrci-hrco:	236.2196			mass flow check	
Refg flow	0.04495	Kg/s (Mr)		calc =	0.043067 Kg/s
Qrc	10618.08	watts			
Qw-Qrc	-439.96	VAR(%):	4.322604		

4. AIR SIDE HEAT BALANCE.

		1st vel	2nd vel
Vel C.F.=	0.88	5	4.4
Ave vel =	4.39	m/s (corrected=Vm)	
Area(Am)=	0.45	m^2	
Airflow =	1.96	m^3/s	
Massflow=	2.54	(Ma,kg/s)	
Ton	-0.47	C	
Toff	-3.28	C	
Tdiff	2.81	C	

Velocity grid measurements

	1:	2:	3:	4:	5:	6:	7:	air mass flo
								Mair=
1:	5	5.1	5.3	5.3	5.2	5	5.1	air flow
2:	5	5.1	5.1	5.2	5.2	5.1	5.2	Vel tun
3:	4.9	4.9	5	5.1	5	4.9	5.2	
4:	4.7	4.2	4.8	5	5	4.2	5	

Ave(Vm)= 4.993 m/s

air dens:	1.295	Kg/m^3	Vh =	0.774	(humid vol)
Qair	7211.3	watts (sensible)			

5. EVAPORATOR HEAT BALANCE.

	out	in	ave	
Evap Press	3.27	3.41	3.34	bar a
S.S.T:	-12.19	-11.07	-11.63	C

Pre expansion valve			Post evaporator		
Trvi =	23.204	C	Tro =	-2.69	C
Prvi =	11.123	bar a	Pro =	3.273	bar a
SST =	27.31		SST =	-12.19	
Subcool	4.11	C	Superheat	9.50	C
hro =	228.13	J/Kg	hro =	407.13	J/Kg

hro-hrvi =	179.00	J/kg			
Refrg flow	0.045	Kg/s			
Qre	8046	watts	Ingress =	10.23	watts
Qre-Ingress:		8036 watts			

6. HEAT INPUTS TO SYSTEM.

	Sensible	latent	total					
Heaters:	5565.0	0.0	5565.0	(Qdry)	Tsurf =	-4.61		
steam:	17.9	1335.4	1352.9	(Qwet)	Cg =	1.864		
Fans:	869.6	0.0	869.6	(Qfan)	E(insln)	1.75		
Ingress:	392.4	43.6	436.0	(Qing)	Area1	27.9	A1dT1	527.0
TOTAL	6844.9	1379.0	8223.4	watts	Area2	27.9	A2dT2	605.5

7. WATER BALANCE.

WATER ADDED

H2O wt	time(min)	rate(kg/s)	
10980	-10		
10450	10	0.000442	
10050	30	0.000333	
9530	50	0.000433	
1450	3600	0.000403	Ms(2)

EVAPORATION RATE

Power in	1417.5	W	A(humid)=	0.8956	m^2
hfg	2576	kJ/Kg	T(makeup)	20	C
hf	84	kJ/kgC	T(bath)	20	C
Losses =	200	watts			
Ms(1)	0.000470	Kg/s			

Water out by coil= 0.000396 kg/s (dH)

Total for 10	3	H2O added =	0.073	kg
min run		H2O evap =	0.085	kg
		H2O on coil =	0.071	kg
		difference	0.007	kg

8. TOTAL TO SENSIBLE HEAT RATIO.

Entering RH:	68.06			T:S ratios	
Entering humidity:	0.00246		T:S(1) =	1.156	(Air-on vs air-off data)
Leaving RH	79.49		T:S(2) =	1.201	(heat input data)
Leaving humidity:	0.002304		T:S(3) =	1.275	(Air-on vs SST-off)
Tsurf =	-4.61		T:S(4) =	1.114	(Qre/Qair)
Heat @SST	0.001311		T:S(5) =	0.936	(air on vs Tsurf)
Heat @Tsurf	0.002555				
hig	2834000	J/Kg		Latent heat	
Cg	1864	J/kgC	Qlat(1) =	1122.8	(humidity difference)
			Qlat(2) =	1379.0	(wet heat input)
			Qlat(3) =	824.5	(Qre-Qair)

pw(SST)=	213.5852	(below zero
pw(Tsurf)	415.3119	

Qair(s)	7211.3
Qair(l)	1122.8
Qair(tot)	8334.1

9. HTC'S

AIR SIDE			REFRIGERANT SIDE				
ha:	66.56	(4fp)	SSTo	-12.1871	Fin Area	36.21	(Afn)
hr:	203.21		Qair:	7211.34	tube A(od)	5.11	(Ap)
hr(corr)=	258.19		1/UA:	0.001421	Area(Ato)	41.32	
Fin eff:	0.83		1/hr.Ap	0.000994	Area(Ap)	4.95	
LMTD:	10.25		1/(ha.Af):	0.000427	Effv Area:	35.16	
LMTD(a)	9.62	include dP					
UA:	703.54						
UAon:	615.31						

7. SUMMARY OF RESULTS. 03/11/93 15:51:00 Version 10

AIR on:	-0.47	C	Evap in:	-10.67	C	Tsurf =	-4.61			Ton-SST:	10.60 C
AIR off:	-3.28	C	Evap out	-2.69	C	Ow	10178	cond water		LMTD	10.25 C
AIR t.d.:	2.81	C	SST:	-11.0716	C	Qrc	10618	refrig (condens)		UA	703.54
air flow:	1.96	m^3/s	refg flow	0.0450	kg/s	Qre	8036	refrig (evap)		UAon	615.31
face vel:	1.98	m/s	cond flow	0.2339	kg/s		tot	sensible	latent	ha:	66.56
RHon:	68.06	%	Hon:	0.00246	kg/kg	Qin	8223	6845	1379	hr:	203.21
RHoff:	79.49	%	Hoff:	0.002304	kg/kg	Qair(tot)	8334	7211	1123	T:S	1.20
										S:T	0.83